Available online at www.sciencedirect.com
ScienceDirect
Tectonophysics 424 (2006) 69–97
TECTONOPHYSICS
www.elsevier.com/locate/tecto

Microfabrics of calcite ultramylonites as records of coaxial and non-coaxial deformation kinematics: Examples from the Rocher de l'Yret shear zone (Western Alps)

Ghislain Trullenque [a,*], Karsten Kunze [b], Renee Heilbronner [a], Holger Stünitz [a], Stefan M. Schmid [a]

[a] *Department of Geosciences, Basel University, Bernoullistr. 30-32, CH-4056 Basel, Switzerland*
[b] *Geological Institute, ETH Zürich, CH-8092 Zürich, Switzerland*

Received 24 September 2004; received in revised form 30 May 2006; accepted 21 June 2006
Available online 10 August 2006

Abstract

Microfabrics were analysed in calcite mylonites from the rim of the Pelvoux massif (Western Alps, France). WNW-directed emplacement of the internal Penninic units onto the Dauphinois domain produced intense deformation of an Eocene-age nummulitic limestone under lower anchizone metamorphic conditions (slightly below 300 °C). Two types of microfabrics developed primarily by dislocation creep accompanied by dynamic recrystallisation in the absence of twinning. Coaxial kinematics are inferred for samples exhibiting grain shape fabrics and textures with orthorhombic symmetry. Their texture (crystallographic preferred orientation, CPO) is characterised by two *c*-axis maxima, symmetrically oriented at 15° from the normal to the macroscopic foliation. Non-coaxial deformation is evident in samples with monoclinic shape fabrics and textures characterised by a single oblique *c*-axis maximum tilted with the sense of shear by about 15°. From the analysis of suitably oriented slip systems for the main texture components under given kinematics it is inferred that the orthorhombic textures, which developed in coaxial kinematics, favour activity of <10–11> and <02–21> slip along the *f* and *r* planes, respectively, with minor contributions of basal-<*a*> slip. In contrast, the monoclinic textures, which developed during simple shear, are most suited for duplex <*a*> slip along the basal plane. The transition between the dominating slip systems for the orthorhombic and monoclinic microfabrics is interpreted to be due to the effects of dynamic recrystallisation upon texture development. Since oblique *c*-axis maxima documented in the literature are most often rotated not with but against the shear sense, calcite textures alone should not be used as unequivocal shear sense indicators, but need to be complemented by microstructural criteria such as shape preferred orientations, grain size estimates and amount of twinning.
© 2006 Elsevier B.V. All rights reserved.

Keywords: Calcite; Microstructure; Crystallographic preferred orientation; Shape preferred orientation; Shear kinematics; Coaxial and non-coaxial deformation; Texture goniometry; CIP

1. Introduction

Microfabrics, i.e. microstructures and textures, are important records of deformation conditions and kinematics in deformed rocks. The term texture refers to

* Corresponding author. Tel.: +41 61 267 3607; fax: +41 61 267 3613.
E-mail address: ghislain.trullenque@unibas.ch (G. Trullenque).

0040-1951/$ - see front matter © 2006 Elsevier B.V. All rights reserved.
doi:10.1016/j.tecto.2006.06.004

crystallographic preferred orientations (CPO) as used in materials sciences (Bunge, 1982). Calcite microfabrics are particularly used to characterise deformation under low-grade metamorphic conditions, where other minerals do not deform by intracrystalline creep but show cataclastic deformation without dynamic recrystallisation. Different texture types were distinguished for "high" or "low" temperature deformation of calcite (Wenk et al., 1987; Leiss and Ullemeyer, 1999; Leiss and Weiss, 2000; Leiss and Molli, 2003).

There has been considerable debate about the interpretation of symmetry vs. asymmetry of calcite textures and their kinematic significance as indicators for pure shear or simple shear deformation (Kern and Wenk, 1983; Wenk et al., 1987; De Bresser, 1989; Ratschbacher et al., 1991; Erskine et al., 1993; Burlini et al., 1998; Leiss et al., 1999; Bestmann et al., 2000; Kurz et al., 2000). Calcite textures in naturally and experimentally deformed rocks often exhibit *c*-axis maxima rotated against the sense of shear (Schmid et al., 1981, 1987; Lafrance et al., 1994; Casey et al., 1998). However, there are also textures reported with *c*-axis maxima either oriented exactly normal to the shear direction (Pieri et al., 2001a,b; Barnhoorn et al., 2004; Oesterling et al., submitted for publication), or slightly rotated with the sense of shear (Lafrance et al., 1994; Bestmann et al., 2000). Because of such ambiguities, Lafrance et al. (1994) questioned the applicability of calcite textures altogether as shear sense criteria. Further confusion arises from inconsistency in defining the sample reference frame, i.e. whether the foliation or the shear zone boundary are taken as the reference plane, all of which are approximately parallel only after large finite shear strain. Textures with *c*-axis maxima normal to the foliation or symmetrically inclined in two conjugate orientations with respect to foliation and lineation have been interpreted as indicating pure shear deformation (Kern and Wenk, 1983; Wenk et al., 1987). This interpretation is ambiguous, as there are also textures reported with *c*-axis patterns of orthorhombic or even axial symmetry from shear zones that show convincing evidence for non-coaxial deformation (e.g. Bestmann et al., 2000). However, the inverse conclusion is certainly applicable, namely that pure shear deformation (of an initially isotropic aggregate) must lead to fabrics with at least orthorhombic symmetry. Analogously, simple shear must result in fabrics that possess at least monoclinic symmetry, but they may have higher (e.g. orthorhombic) symmetry. Torsion experiments (Pieri et al., 2001a,b; Barnhoorn et al., 2004) demonstrated that one and the same simple shear kinematics and identical deformation conditions result in calcite textures with monoclinic symmetry at low strain, which evolve into textures with either orthorhombic or monoclinic symmetry at large strain.

Apart from texture, a wide variety of microstructural features are potential kinematic indicators in deformed rocks (e.g. Passchier and Trouw, 1996). In monophase aggregates, it is particularly the grain shape fabric, here referred to as shape preferred orientation (SPO). An orthorhombic SPO is generally indicative of dominantly coaxial deformation whereas a monoclinic SPO is indicative of dominantly non-coaxial deformation (for calcite see: Schmid et al., 1987; Lafrance et al., 1994; Bestmann et al., 2000; Pieri et al., 2001a,b). Torsion experiments (Barnhoorn et al., 2004) have demonstrated that a monoclinic SPO is established after low strain ($\gamma \sim 1$) and remains stable under shear deformation up to large strain.

A number of recent contributions (Herwegh and Kunze, 2002; Herwegh and Berger, 2003) have demonstrated that the presence of very small amounts of nanometer- and micron-scale second phase particles was of crucial importance regarding the microfabric evolution of calcite mylonites. Herwegh and Kunze (2002) concluded that differences in CPO and SPO geometry (symmetric vs. oblique) in calcite mylonites sampled within the Helvetic Alps are related to different amounts of second phase particles, as they influence the balance between intragranular deformation and dynamic recrystallisation.

This paper describes microstructures and textures analysed in samples of naturally deformed limestone mylonites collected along two profiles across the Rocher de l'Yret shear zone at the rim of the Pelvoux massif (Western Alps). Microfabrics and field evidence clearly indicate distinguishable cases for simple and pure shear dominated deformation for the two sample series, respectively, which should have occurred simultaneously under the same temperature and comparable strain rates. It is concluded that the systematic differences observed in microstructure and texture are due to different deformation paths. Hence the two series of samples may serve as prototypes of distinct types of textures that are indicative of the kinematics of deformation.

2. Geological framework of the study area

2.1. Regional setting

The Rocher de l'Yret Shear Zone (RYSZ), situated at the eastern rim of the Pelvoux massif (Western Alps, France; Fig. 1), separates the Dauphinois domain from the Penninic units and forms part of the Pennine/Penninic Front (Merle and Brun, 1984; Mosar et al., 1996; Bagnoud et al., 1998) also referred to as Pennine/Penninic Frontal

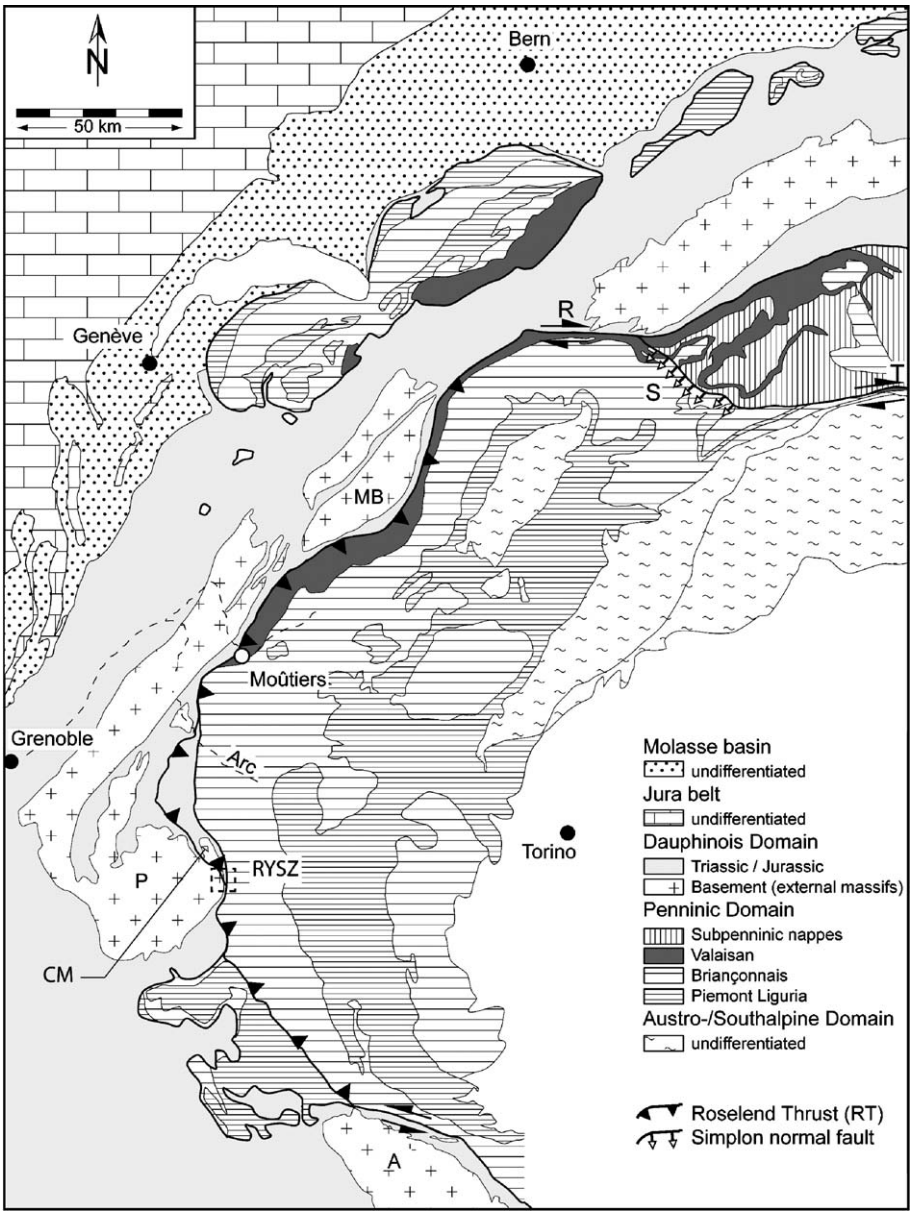

Fig. 1. Simplified geological overview of the arc of the Western Alps (A: Argentera massif, CM: Combeynot massif, MB: Mont Blanc massif, P: Pelvoux massif, R: Rhone-Simplon line, S: Simplon normal fault, T: Tonale line, RYSZ: Rocher de l'Yret shear zone; after Froitzheim et al., 1996; Ceriani et al., 2001).

thrust (Spencer, 1992; Seward and Mancktelow, 1994; Bürgisser and Ford, 1998). According to Ceriani et al. (2001), this thrust formerly represented a suture zone between Dauphinois and Briançonnais/Subbriançonnais, active during Eocene times and related to the subduction of the Valaisan Ocean. The Valaisan oceanic domain was closed in sinistral transpression, associated with a top to the north sense of movement. During a second deformation stage (Oligo–Miocene), WNW-directed thrusting along the entire Western Alps on a major out-of-sequence thrust, the Roselend thrust, completely reworked the Penninic front. In particular, calcite mylonites were formed in Eocene sediments (nummulitic limestone) on top of a regional unconformity, which cuts across the Jurassic sediments into the basement and is defined by the deposition of a detrital calcitic conglomerate.

2.2. Temperature conditions during deformation

The degree of Alpine metamorphic overprint of the eastern rim of the Pelvoux massif, as estimated by Aprahamian (1974, 1988) by means of illite crystallinity

(IC) measurements, occurred under epizonal conditions (IC <2.8 for the RYSZ). Furthermore, temperatures can indirectly be derived from a contoured zircon fission track isochron map of the Western Alps compiled by Fuegenschuh and Schmid (2003). The whole eastern rim of the Pelvoux massif is characterised by zircon fission track ages older than 60 My, indicating that the corresponding rocks had not been exposed to temperatures above the upper limit of the zircon partial annealing zone, i.e. 320 °C (Tagami et al., 1998), for 60 My. Zircon fission track data from the Briançonnais and Dauphinois domains, immediately south of the RYSZ (Seward et al., 1999), yielded ages older than 100 My, which clearly excludes metamorphic temperatures above 320 °C during the Tertiary. Hence, temperatures must have been around 300 °C or even slightly below around the whole eastern rim of the Pelvoux massif. Preliminary results based on new IC data and fluid inclusion analyses indicate low anchizonal metamorphic conditions (Potel, pers. comm.), putting the epizonal conditions proposed by Aprahamian (1974, 1988) again under question.

2.3. Structural setting

At the eastern rim of the Pelvoux massif, the Roselend thrust (RT) enters the Mesozoic cover of the external massifs. It thrusts the Combeynot massif (CM) together with its Eocene sedimentary cover over the Pelvoux massif towards the West (Fig. 1). Near the outcrop investigated in this study, the Combeynot massif joins the RYSZ, which is a km-wide shear zone that represents the RT in this area.

The RYSZ is an imbricate structure consisting of two large slices of the Pelvoux massif, the lower "Grangettes" slice, and the upper "Montagnolle" slice (Gignoux and Moret, 1938; Gidon, 1954; Gidon, 1979; Beach, 1981; Ford, 1996). Butler (1992) has described WNW-directed shearing of nummulitic limestones in a basement/cover imbricate structure forming the Rocher de l'Yret summit

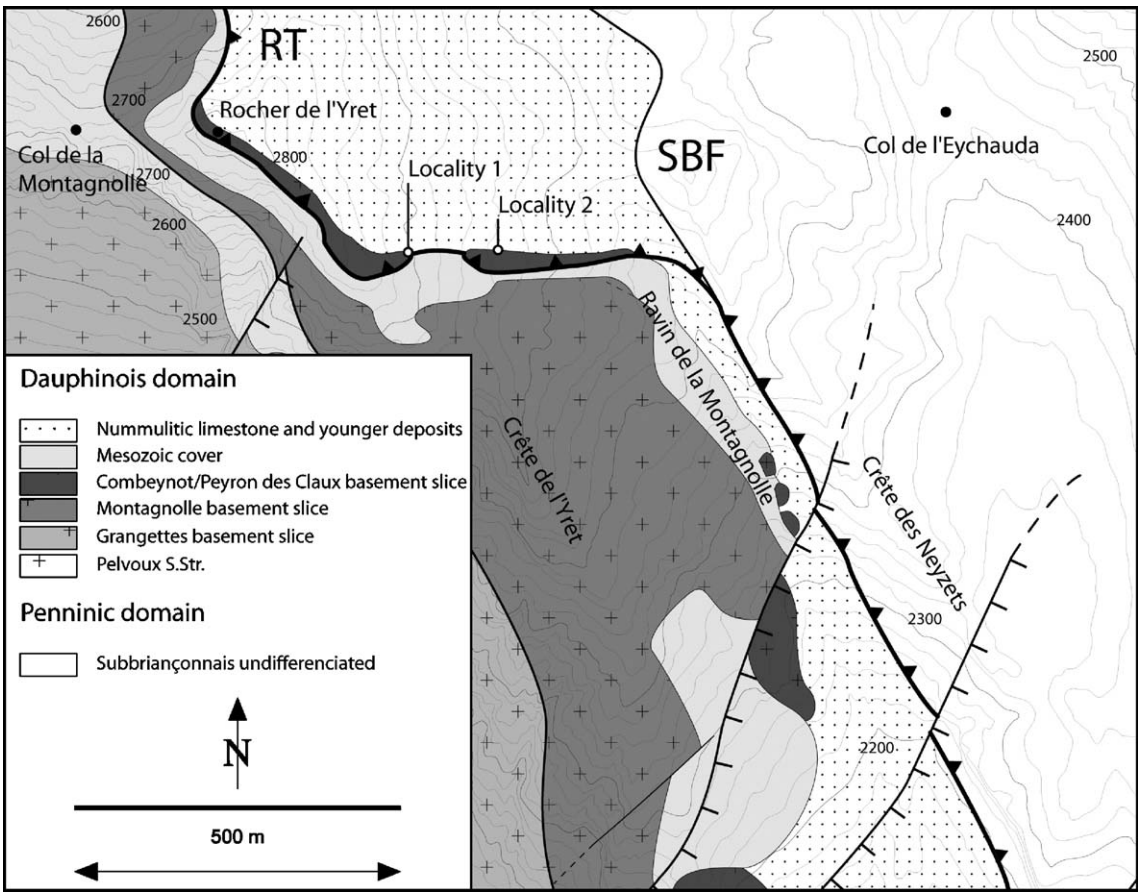

Fig. 2. Detailed geological map of the sampling area around the Rocher de l'Yret shear zone (RYSZ) after field mapping (Trullenque, 2005); sampling localities 1 and 2 are marked.

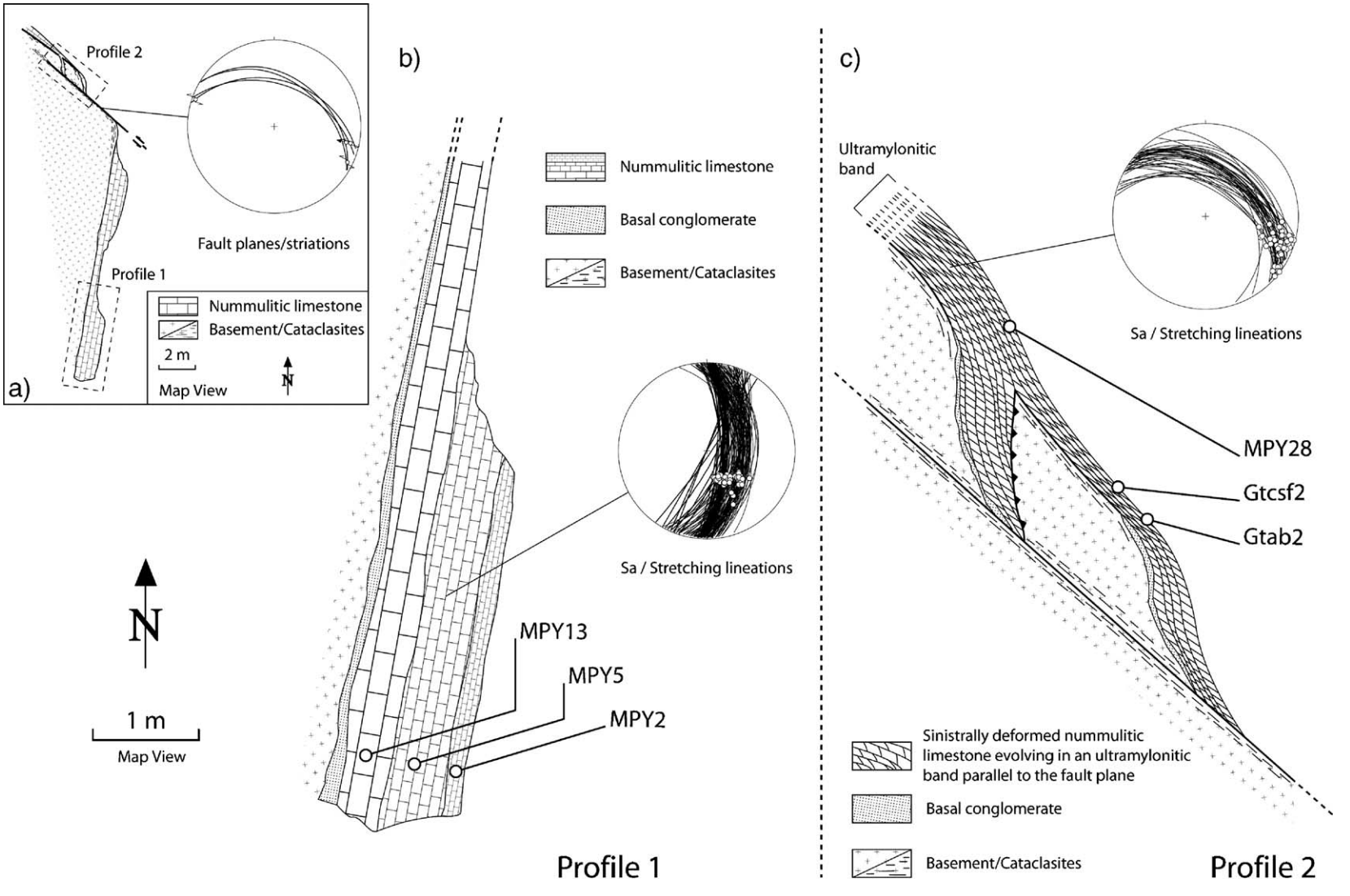

Fig. 3. a) Structural scheme of the investigated outcrop at sampling locality 1. Fault plane orientations with striations of the main strike-slip zone are reported. b) Map of profile 1 with location of samples MPY13, MPY5, MPY2; macroscopic foliations Sa with stretching lineations of nummulitic limestone. c) Map of profile 2 with location of samples Gtab2, Gtcsf2 and MPY28; macroscopic foliations Sa with stretching lineations of nummulitic limestone.

(Fig. 2). According to own regional studies (Trullenque, 2005), this summit consists of a third and very thin basement slice, together with its Eocene-age stratigraphic cover, which represents the calcite mylonites investigated by this study. Thrusting along the RT additionally led to local strike-slip faults affecting these basement-cover boudins.

Most of the samples for this study were taken from an outcrop (locality 1 in Fig. 2) situated within the top-most parts of the RYSZ. It exposes a layer of mylonitised nummulitic limestone that was originally in stratigraphic contact with an isolated basement boudin. At its northern edge, this basement-cover boudin is cut by a sinistral strike-slip zone (Fig. 3a). Lineations and associated shear sense criteria indicate top-WNW shearing over the entire area of the outcrop. Deformation inside the crystalline basement was accommodated by cataclastic faulting and/or flow (Fig. 4a, b), which is consistent with the very low-grade metamorphic conditions, while the nummulitic limestone underwent crystal–plastic deformation.

The main limestone layer is accessible over a horizontal distance of about 20 m striking NNE–SSW. Its mylonitic to ultramylonitic foliation is parallel to internal bedding and to the original stratigraphic contact with the basement boudin. The layer reaches a maximum thickness of 110 cm at the southern termination of the outcrop. Abundant nummulites, several millimetres in size, are preserved in the bottom 30 cm of the sheared limestone layer. In the vicinity to the basal conglomerate it also contains a significant portion of detrital quartz. This quartz–calcite-mixture develops a strong stretching lineation. Progressive development of a mylonitic foliation parallel to the bedding plane can be observed at increasing distance from the basement and towards the ESE. Decreasing amounts of recognizable nummulite shells correlate with increasing degree of dynamic recrystallisation in calcite, which is also interpreted as a strong gradient in finite strain normal to foliation. In this part of the outcrop sampling was carried out along a traverse normal to the foliation (profile 1, Fig. 3b).

The strike-slip zone exposed in the northern part of the outcrop (Fig. 3a, c) is associated with the formation of a basement/cover imbricate structure. Along the strain gradient normal to the strike-slip fault, which cataclastically dissects the basement units, the limestone is intensively sheared in a sinistral sense and the upper levels of the layer are progressively bent around the basement slice.

Again, progressive disappearance of macroscopically recognizable nummulite shelves normal to the strike of the limestone indicates that this unit is affected by intensive dynamic recrystallisation. The limestone evolves into an ultramylonitic band showing numerous isoclinal folds, together with a WNW oriented stretching lineation defined by quartz grains.

All samples have been taken at the upper part of the limestone and ultramylonitic band in an orientation subparallel to the one of the strike-slip fault dissecting the basement unit (profile 2, Fig. 3c).

The transition in orientation of both foliations and stretching lineations is rather gradual between the locations of profile 1 (steeply plunging stretching lineation) and profile 2 (mostly horizontal or shallowly plunging stretching lineation) and suggests that deformation of the limestone layer was coeval in profiles 1 and 2.

A paleostress analysis was performed for a set of 124 co-genetic fault planes dissecting basement boudins and their Eocene cover. This analysis was carried out using Tectonic VB software [1] including inversion methods (Angelier and Mechler, 1977). The results (Fig. 5) show average orientations of σ1 at N264/10 and of σ3 at N154/60, which are considered to be representative for the

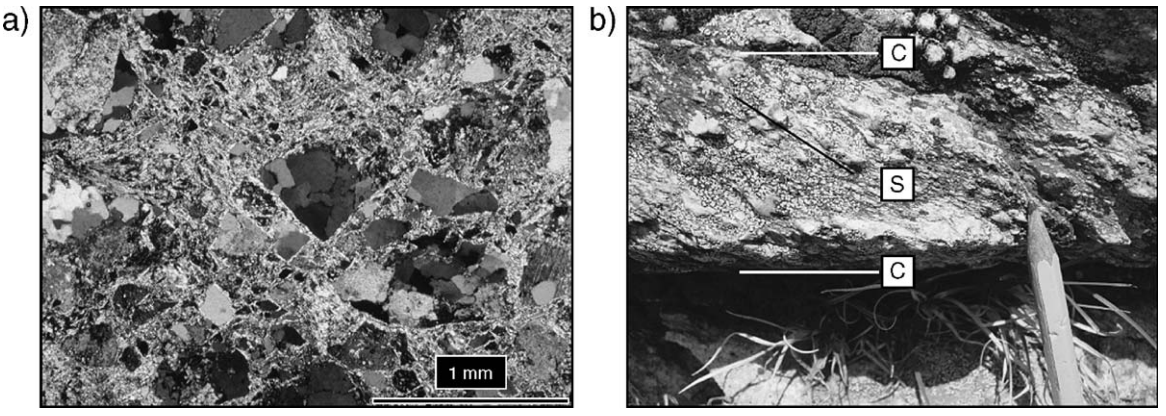

Fig. 4. a) Photomicrograph of the granitic basement cataclastic rock. Large angular patches are dominantly composed of quartz grains and quartz aggregates. b) Close view of the granitic basement cataclasite along the main strike-slip fault plane.

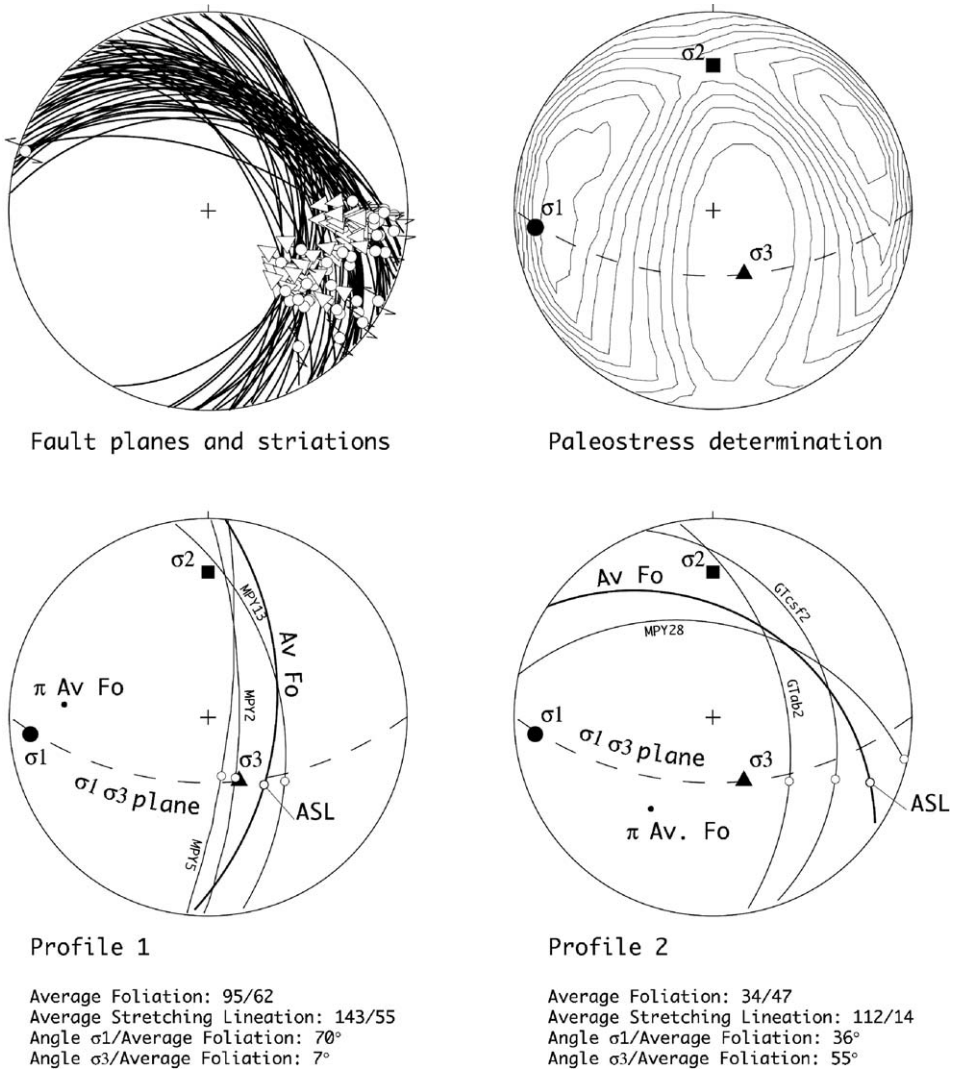

Fig. 5. Paleostress analysis in the basement adjacent to limestone mylonites: P, B and T axes derived from 124 individual fault planes; average orientation of the principal stress axes σ1 (N264/10), σ2 (N0/27), σ3 (N154/60) are superposed over projections of macroscopic foliations (labeled great circles) and stretching lineations (open balls) from profiles 1 and 2 (on average and for the studied samples). Contours of σ1, σ2 and σ3 are given in multiples of a uniform distribution with a contour interval of 0.3.

orientation of the bulk stress tensor at a larger scale in the whole RYSZ. Throughout the outcrop, foliation planes roughly intersect in the intermediate stress axis σ2, while stretching lineations are about perpendicular to it within the σ1–σ3 plane (Fig. 5). For profile 1, the average stretching lineation falls close to σ3 while the average foliation is oriented subnormal to σ1. This kinematic framework is compatible with coaxial deformation.

For the ultramylonitic band of profile 2, σ1 and σ3 fall at intermediate (roughly 45°) angles to the average foliation and to the average stretching lineation of the mylonitic layer (Fig. 5). This kinematic framework is indicative of non-coaxial deformation. If deformation were restricted to plane strain, for which we do not have ultimately decisive indications, then profiles 1 and 2 could be related to pure shear respectively simple shear dominated kinematics.

3. Methods of investigation

Samples were cut normal to the macroscopic foliation (Sa) and parallel to the stretching lineation (*XZ* sections). Approximately 2 μm thick ultrathin sections showing first order grey in calcite in crossed polarised light were prepared for microstructural analysis and for mapping of *c*-axis orientations by computer integrated polarisation

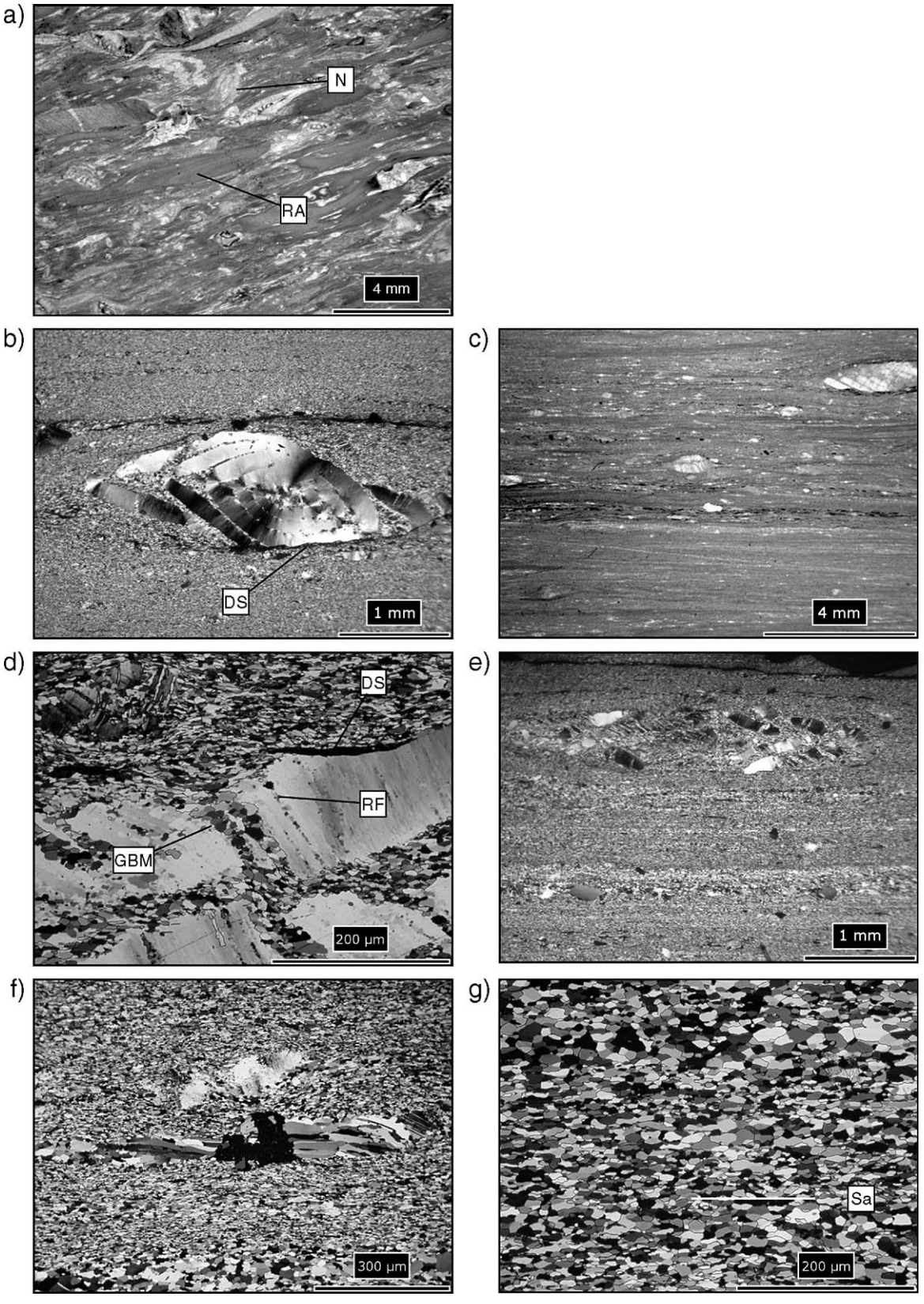
a)
N
RA
4 mm
b)
DS
1 mm
c)
4 mm
d)
DS
RF
GBM
200 µm
e)
1 mm
f)
300 µm
g)
Sa
200 µm

(CIP) microscopy (Panozzo Heilbronner and Pauli, 1993, 1994). Vectorisation of grain boundaries was performed on digital micrographs using a combination of NIH Image [2] and own software. On average, about 3500 particles were evaluated per sample to determine their SPO and grain size distributions. The preferred orientation of the grain long axes was determined using the PAROR method, while the preferred orientation of grain boundary surfaces was analysed using the program SURFOR (Panozzo, 1983, 1984). The determination of particle grain sizes was performed using the program STRIPSTAR [3].

Pole figures were measured with a SIEMENS D5000 X-ray texture goniometer in reflexion and transmission modes for three crystallographic planes (*r* {10–14}, *a* {11–20} and *h* {20–22}) for each sample. Lattice planes and directions are designated here by Miller–Bravais hexagonal indices referring to the structural hexagonal unit cell with axial ratio $c/a=3.419$ as classified by Wyckoff (1920). Empirical corrections for defocusing in reflection mode and for scattering volume in transmission mode were applied before merging into complete pole figures. The orientation distribution function (ODF) was calculated using both MENTEX (Schaeben et al., 1990) and BEARTEX-WIMV (Wenk et al., 1998) software, and selected ODF sections are displayed by intensity contour plots. The quality of the ODF calculations was consistently satisfactory as verified by confidence parameters (difference pole figures, RP values, convergence rate) provided by the respective software packages. The applied convention for Euler angles (ψ_1, Φ, ψ_2) relates to the one (φ_1, Φ, φ_2) defined by Casey (1981, his Fig. 3) and Bunge (1982) by $\psi_1=\varphi_1$ and $\psi_2=\varphi_2+90°$, as the crystal coordinate axis X_c is placed here parallel to $+a$ instead of *m*. Pole figures were recalculated from the ODF for the three measured reflections and additionally for the basal (0001) and the *f* {01–12} planes, for the inferred slip directions *sd1* <10–11> and *sd2* <02–21>, and so are inverse pole figures for particular specimen directions. All pole figures and inverse pole figures were treated with inversion symmetry except for the recalculated $+a$ <−1–120> and $-a$ <11–20> (non-reduced) pole figures. All figures are displayed using equal area projections of the upper hemisphere.

The measured orientation distributions were compared to idealised textures, which are modelled to be composed of a few components around fixed ideal crystal orientations using Gaussian standard distributions of constant and isotropic angular spread (half width of 40°; software package BEARTEX, Wenk et al., 1998). These model textures could be regarded as first approximation for a complete component fit according to the methods developed by Helming et al. (1994). Pole figures, inverse pole figures and ODF sections of these model textures were displayed analogously to those of the corresponding samples.

4. Microstructure and texture of nummulitic limestone mylonites

Microstructures and textures in limestone mylonites were quantitatively described for about 130 collected and analysed specimens along the Roselend thrust (Trullenque, 2005). In this huge data set, textural and microstructural characteristics are largely repetitive and cluster around two similar but distinct types, which are represented here by samples from profiles 1 and 2 of locality 1. Some other cases are exemplified here by one sample (Sa1a4) from locality 2. The protolith prior to shear zone formation is characterised by one weakly deformed sample (245a), which contains the sedimentary components still preserved.

Texture strength and degree of fabric anisotropy generally increase with distance from the basement, which will be interpreted also as gradients in finite strain and amount of recrystallisation. The three samples selected for each of the two profiles characterise these gradients.

4.1. Protolith

4.1.1. Sample 245a (Fig. 6a)

The sample was collected south of the investigated shear zone and preserves an association of nummulites, echinoderma fragments and red algae. Two types of components were observed in the thin section. The first type consists of nummulite and echinoderm fragments

Fig. 6. Photomicrographs of different limestone samples indicating mostly coaxial deformation (profile 1). Photomicrographs were taken from standard thin sections (30 μm thick) in transmitted light without polarisers (a, c), and from ultrathin sections (2 μm thick) in cross-polarised transmitted light (b, d, e, f, g). All sections are oriented normal to foliation and parallel to lineation (horizontal). a) Nummulitic limestone protolith (sample 245a), weakly deformed prior to shear zone formation. Note the association of nummulites (N) and red algae (RA). b, c) Sample MPY13 shows a strong horizontal Sa foliation and dissolution surfaces (DS) subparallel to Sa. The original radial *c*-axis distribution around the nummulite shell is still preserved. d, e) Sample MPY5 shows a horizontally elongated nummulite shell. Microstructural features indicate grain boundary migration (GBM), rotation recrystallisation and pressure solution processes that have been active simultaneously. Recrystallisation festoons (RF) normal to the nummulite rim. f, g) Sample MPY2 is an entirely recrystallised limestone with a grain shape preferred orientation horizontal (parallel to Sa) and symmetric calcite pressures fringes developed at the rim of detrital quartz grains.

whose size varies between 0.4 and 3.2 mm. Nummulite species *N. garnieri and N. fabianii* were identified. The shell of these organisms is made up of several rims of fibrous calcite showing a typical radial *c*-axis pattern. The echinoderm fragments are rounded calcite single crystals and constitute 20% of the rock. The second type of components consists of red algae mats. They appear as elongated patches with an average aspect ratio higher than 10:1. Their internal structure shows micritic calcite grains with very lobate boundaries and grain size ranging between 2 and 4 μm. These algae mats form between 50 and 60% of the rock. The rest of the rock

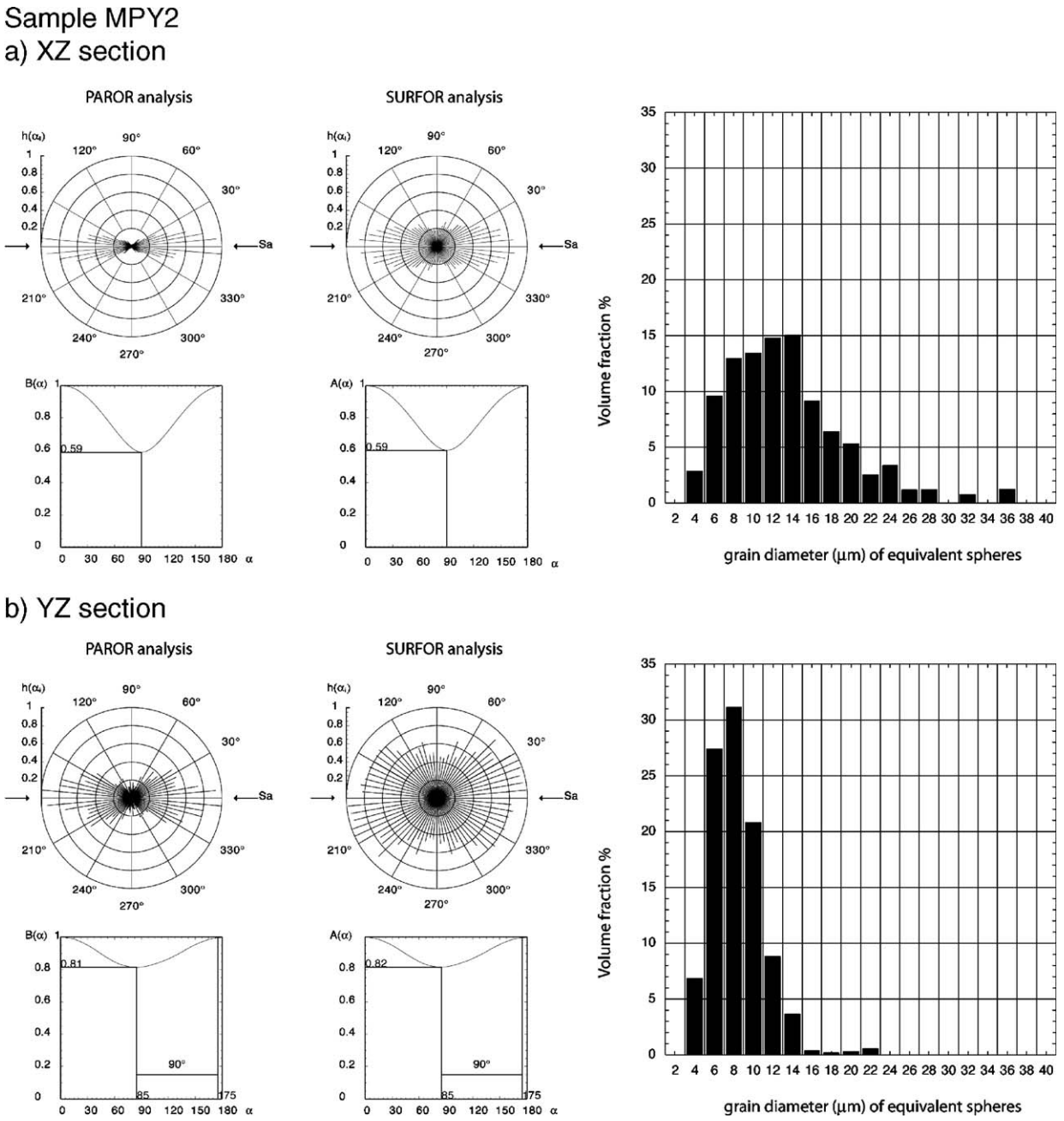

Fig. 7. Microstructural analysis of mylonite sample MPY2 indicating coaxial deformation: The average grain shape ellipsoid is triaxial and parallel to the structural reference frame. Rose diagrams for orientation distributions of particle long axes (PAROR) and of grain boundaries (SURFOR). Histograms of volume-weighted grain size distributions. a) *XZ* section, i.e. perpendicular to foliation and parallel to stretching lineation. b) *YZ* section, i.e. perpendicular to both foliation and stretching lineation.

consists of calcitic matrix material, as well as of detrital mica, quartz, or mud pellets (Fig. 6a).

Most of the clearly visible shape fabric anisotropy is attributed to primary sedimentary processes including compaction and not to tectonic deformation during thrusting. Thus sample 245a is considered a typical protolith for the mylonites described below. It shows a texture that is very close to uniform, with faint preferred orientations of *a*-axes perpendicular to and *c*-axes within the bedding plane (Fig. 8, top). A very similar texture was observed in micritic Solnhofen limestone and attributed to passive alignment of calcite grains with their *c*-axes slightly preferred into the bedding plane (Wenk et al., 1973; Casey et al., 1998).

4.2. Profile 1

Below we describe progressive deformation in three samples collected along profile 1 across the southern part of locality 1 (Fig. 3b).

4.2.1. Sample MPY13 (Fig. 6b,c)

This sample shows a protomylonitic fabric, and dynamic recrystallisation affected all the biogenic components. The recrystallisation microstructures are heterogeneous, because the extent of their development is sensitive to the initial structure of the components.

Nummulites and echinoderm fragments typically show a “core and mantle” structure. New grains were

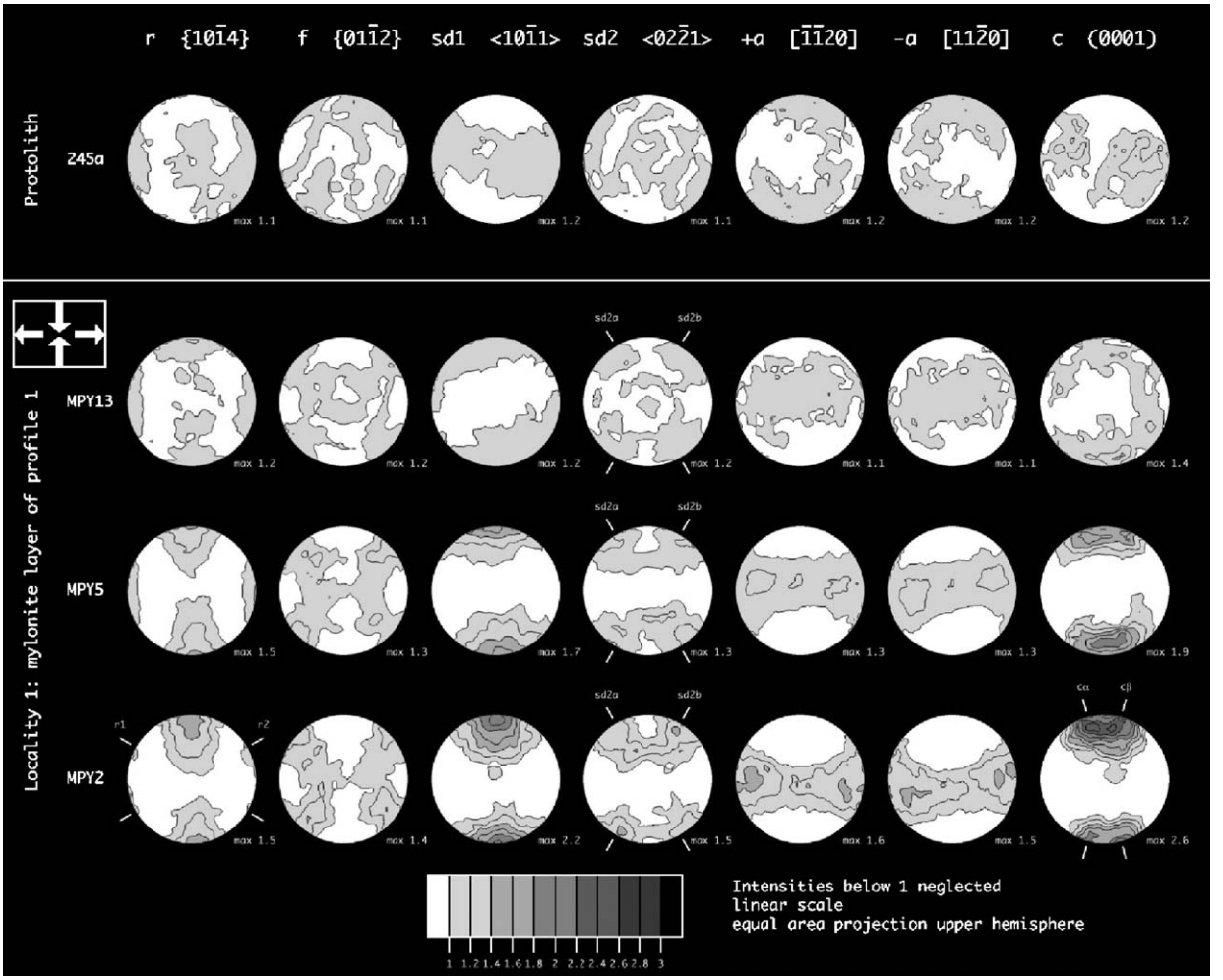

Fig. 8. Texture evolution from the protolith (sample 245a) to mylonites across the limestone layer (profile 1). The protolith shows nearly uniform distributions, which are axial symmetric with faint maxima of *a*-axes perpendicular and of *c*-axes parallel to the bedding plane (S0). The three samples from profile 1 show similar textures of increasing strength with increasing degree of mylonitisation (sorted from top to bottom). Bulk textures obtained by X-ray texture goniometry, all pole figures calculated from the ODF. Pole figure contours are given in multiples of a uniform distribution with a contour interval of 0.2. Intensities below 1 are neglected. The projection is perpendicular to the macroscopic foliation and the stretching lineation is horizontal in the projection plane, equal area projection of upper hemisphere.

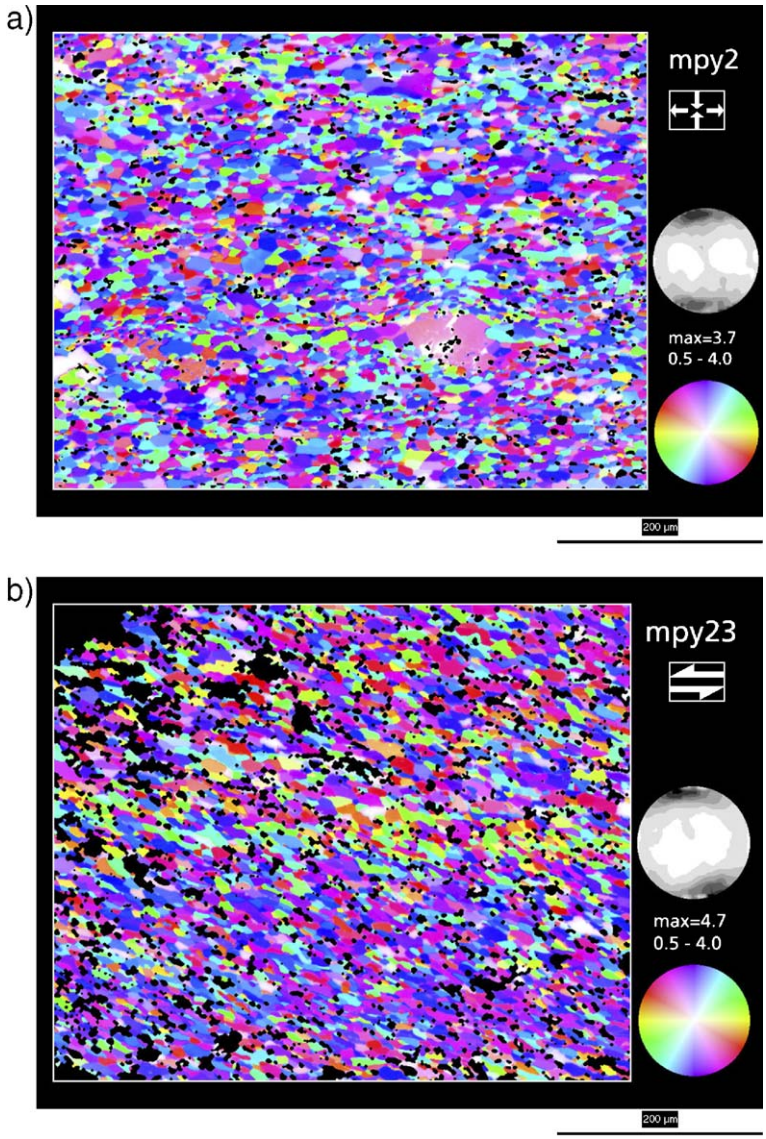

Fig. 9. Computer Integrated Polarisation (CIP) images and derived *c*-axis distributions. Colour look-up table stereogram at lower right. Contours of the *c*-axis pole figure given in multiples of uniform distribution with intervals of 0.5. Specimen orientation as above perpendicular to macroscopic foliation Sa, stretching lineation is horizontal. Holes in the thin-section together with areas of non-constant thickness have been masked using black colour and were not taken into account in the *c*-axis pole figure calculation. a) sample MPY2; b) sample MPY28, sinistral sense of shear.

produced by progressive subgrain rotation in echinoderm porphyroclasts. The internal structure in some nummulites is well preserved and still shows the radial *c*-axis pattern. Echinoderms are more competent than the surrounding fine-grained matrix and were fragmented by fracturing as well as deformed by twinning. Some 10% of the area contains nummulites and echinoderms that are still preserved.

The outer surfaces of nummulites are commonly oriented parallel to foliation. Dark outlines marked by relatively insoluble fine grained minerals (hematite, chlorite, micas) are interpreted as remnants of dissolved material indicating that pressure solution has also contributed to the deformation of these calcite rocks. Some external rims of the nummulites are fragmented during progressive deformation. Where fragmentation occurs, the internal parts of the nummulite shells show a greater degree of dynamic recrystallisation.

4.2.2. Sample MPY5 (Fig. 6d,e)

The microstructure of this sample is characterised by further reduced volume fraction of initial

components due to progressive deformation accompanied by dynamic recrystallisation. Pressure solution was also active, evident by locally dissolved nummulite and echinoderm fragments. Deformation affected the entire nummulite shells. The calcite fibres of the nummulite shells show lobate boundaries with bulges into neighbouring crystals, indicating grain boundary migration. Usually, bulges evolve into festoons of new grains along the fragments. Some of the fibres and their radial *c*-axis patterns are partially preserved. Nummulite shell aggregates are elongated parallel to lineation. The boundaries of primary twins in echinoderms are lobate indicating twin boundary migration. In some places, such twins are bent or overprinted by a second set of deformation twins. The percentage of nummulite and echinoderm fragments has been estimated at no more than 6%, the red algae mats constitute 20% of the rock.

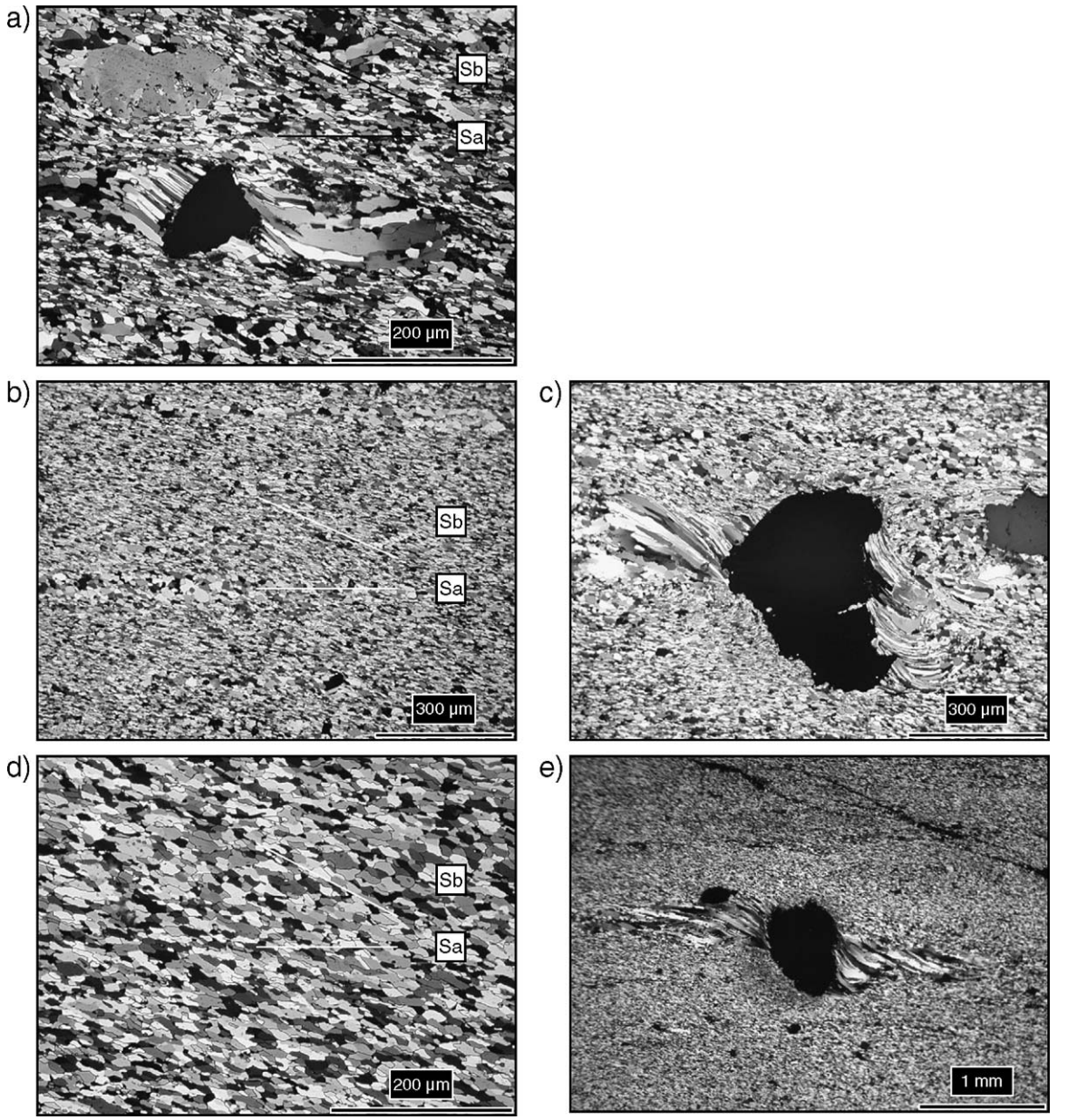

Fig. 10. Photomicrographs of samples indicating non-coaxial deformation, taken from ultrathin sections in cross-polarised light. a) Sample Gtab2; b, c) sample Gtcsf2; d, e) sample MPY28. Asymmetric calcite pressure fringes developed at the rim of detrital quartz grains (a, c and e). Oblique grain shape preferred orientation (Sb) consistent with sinistral sense of shearing in the rock (a, b and d).

4.2.3. Sample MPY2 (Fig. 6f,g)

The main microstructural difference with respect to sample MPY5 is the lack of any relict nummulite shells. The grains of the dynamically recrystallised matrix are completely free of deformation twins and show slightly lobate boundaries. They occupy more than 90% of the

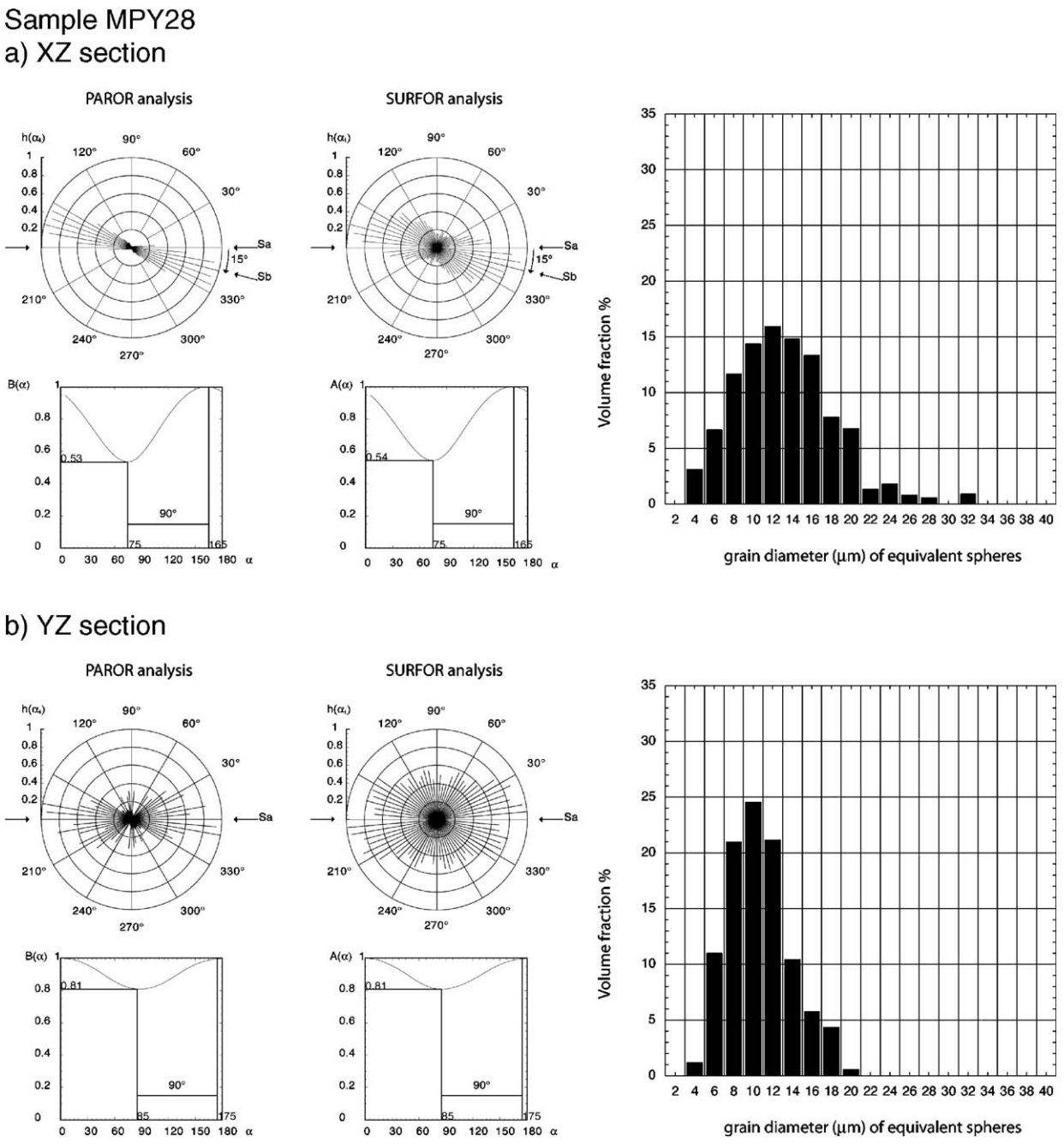

Fig. 11. Microstructural analysis of mylonite sample MPY28 indicating non-coaxial deformation: The average grain shape ellipsoid is triaxial and oblique to the structural reference frame. Same representation as Fig. 7. The grain size distributions show no major differences compared to sample MPY2. a) *XZ* section, i.e. perpendicular to foliation and parallel to lineation. Average grain long axis inclined by 15° to Sa, compatible with sinistral shearing. b) *YZ* section, i.e. perpendicular to both foliation and lineation. Note the slight flattening of the grain shape.

rock. Most pressure shadows filled with calcite fibres around detrital quartz grains are symmetrically developed with respect to the foliation.

4.2.4. SPO analysis (Fig. 7)

The SPO of the recrystallised matrix is similar in all three samples; therefore it is shown here only for sample MPY2. *X–Z* sections of the matrix grains show a strong SPO parallel to the foliation with an average aspect ratio of 0.59 and a grain size mode of 12 μm. *Y–Z* sections show SPO with the average long axis also parallel to foliation, an average aspect ratio of 0.81 and a grain size mode of 8 μm. In combination, the average grain shape ellipsoid is aligned parallel to the structural reference system *XYZ* and plots near the diagonal in a Flinn-type diagram with $K \sim 1.1$ indicating a slightly prolate grain shape. The microstructure of the dynamically recrystallised matrix displays an orthorhombic symmetry with respect to foliation and lineation (Fig. 7).

4.2.5. Texture analysis (Fig. 8)

X-ray texture analysis reveals a similar texture type for all three samples of profile 1, but with strength increasing with increasing distance from the basement. The weak texture of sample MPY13 is significantly different from that of the protolith sample 245a. The pole figures display weak maxima of *c*-axes normal to foliation and *a*-axes distributed along girdles parallel to the foliation (Fig. 8).

In closer detail, pole figure maxima are elongated with some preference of rotations around the foliation normal, indicated by girdles and small circles in some pole figures. The *c*-axis pole figure of the most recrystallised sample (MPY2) shows two distinct maxima (cα and cβ) at the

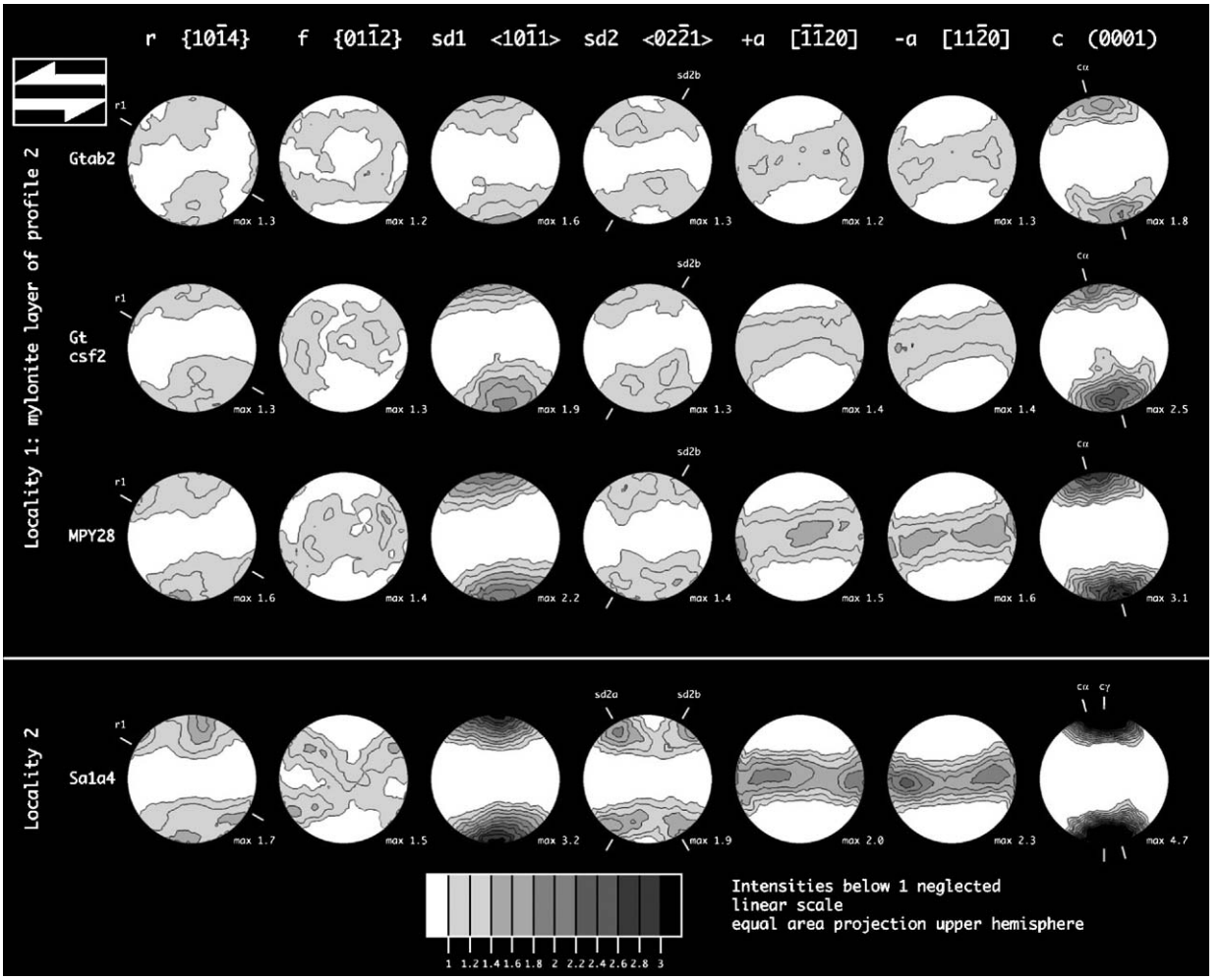

Fig. 12. Texture evolution in the ultramylonitic band (profile 2). Foliation and stretching lineation are horizontal, sinistral sense of shear. Same representation as in Fig. 8. Sample Sa1a4 originates from locality 2 (Fig. 2) and represents intermediate strain kinematics.

periphery of the pole figure, symmetrically oriented at 15° from *Z*. The CIP *c*-axis pole figure of the dynamically recrystallised matrix shows a similarly shaped but stronger maximum normal to the foliation (Fig. 9a). All textures are characterised by orthorhombic sample symmetry, and the non-reduced $+a$ and $-a$ pole figures are approximately identical. The overall patterns are slightly asymmetric relative to the structural reference system by some minor rotations around the lineation, which may be attributed to misalignments with respect to the foliation plane during specimen collection and preparation.

4.3. Profile 2

Below we describe progressive deformation along profile 2 across the sinistral shear zone in the northern part of the outcrop at locality 1 (Fig. 3c). These rocks were deformed under the same P–T conditions as the ones from profile 1. The specific samples were selected to match pair wise those from profile 1 in terms of the extent of dynamic recrystallisation and of texture strength.

4.3.1. Sample Gtab2 (Fig. 10a)

The dynamically recrystallised matrix possesses an inhomogeneous grain size distribution, where diffuse patches of very fine grain size result from red algae remnants. While the grain size distributions are comparable between this sample and sample MPY13 from profile 1, the SPO of their dynamically recrystallised grains is different. The asymmetric SPO is oblique to the macroscopic foliation and consistent with sinistral shearing of the rock which is further confirmed by asymmetric calcite pressure shadows developed at the rim of detrital quartz grains (Fig. 10).

4.3.2. Sample Gtcsf2 (Fig. 10b,c)

In this sample the volume fraction of recrystallised grains, and presumably also strain intensity, is similar to that of sample MPY5 from profile 1. The matrix of this sample shows a clearly oblique SPO compatible with sinistral shearing, further confirmed by asymmetric calcite pressure shadows developed at the rim of detrital quartz grains.

4.3.3. Sample MPY28 (Fig. 10d,e)

The microstructure is dominated by S–C-structures. The secondary foliation Sb is at 30° to the primary foliation Sa, and calcite fibres at the rim of detrital quartz grains show a clear asymmetry consistent with sinistral shearing of the rock. There are no deformation twins in the recrystallised matrix.

4.3.4. SPO analysis (Fig. 11)

The SPO of the recrystallised matrix is similar in all three samples; therefore it is shown here only for sample MPY28. In the *X*–*Z* section grains have an average aspect ratio of 0.53 with preferential elongation at 15° to the foliation. This SPO angle is only half the angle of Sb to Sa, which was intuitively estimated from the micrographs of Fig. 10. This indicates some bias towards grain boundaries instead of grain long axes in the visual determination of Sb. The grain size distribution has a mode of 12 μm. The measurements in the *Y*–*Z* section indicate flattening of the grains normal to the foliation with average aspect ratio of 0.81. In combination, the average grain shape ellipsoid plots near the diagonal in a Flinn-type diagram with $K \sim 1.2$ indicating a slightly prolate grain shape. Its longest and shortest axes lie in the *X*–*Z* plane and make an angle of 15° to the structural reference frame given by mylonitic foliation and lineation (Fig. 11).

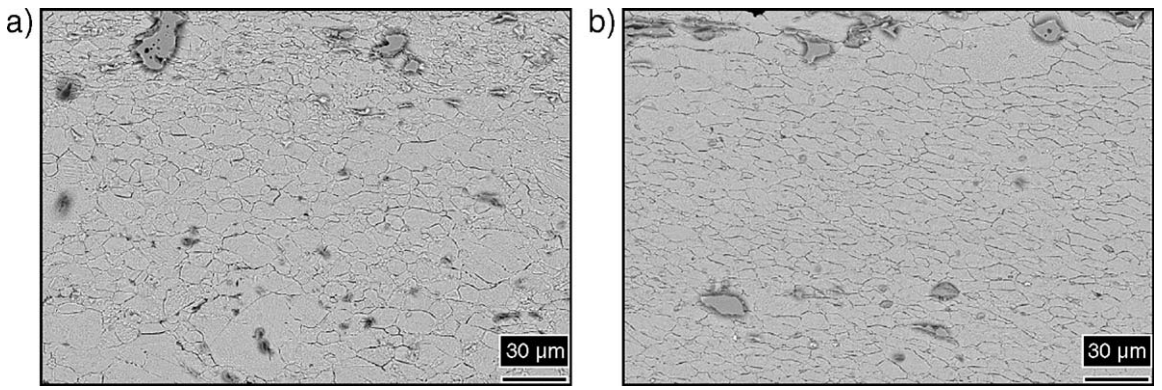

Fig. 13. SEM images (BSE mode, 20 kV acceleration voltage) of typical shape fabrics of sample MPY2 (a) and MPY28 (b). Samples were etched according to the technique described by Herwegh (2000). Light grey: Calcite; darker equant grains: Quartz; darker elongate grains: White micas. Second phase particles do not control the shape of calcite grains.

4.3.5. Texture analysis (Fig. 12)

As in the sample series of profile 1 (Fig. 8), the three samples possess textures of similar type, but with increasing strength again with increasing distance to the basement. The weakest texture of sample Gtab2 has similarly low maxima as sample MPY13, though they are strong enough to distinguish it from MPY13 as well as from the protolith sample 245a. In difference to profile 1, the textures of profile 2 are asymmetric with reference to foliation and lineation, i.e. *c*-axis maxima are at 15° from the foliation normal towards the lineation, and girdles of *a*-axes are similarly inclined to the foliation by counter clockwise rotation of 15° about the structural *Y*-axis. Corresponding asymmetries are particularly visible in the *r* and the *sd2* pole figures. In reasonable approximation, all pole figures contain a two-fold rotational symmetry about the structural *Y*-axis (Fig. 12).

The pole figures of the most recrystallised sample MPY28 show considerably stronger maxima compared to the other two samples of profile 2. The poles to the *r* planes show one maximum close to *Z* and another one at position labelled "r1". The pole figure for the *sd2* slip direction shows two maxima symmetrically oriented with respect to the foliation but with different intensities. Along the girdle distributions of the *a*-axes, the $+a$ direction has the maximum in the projection centre, while the $-a$ direction shows two maxima oppositely

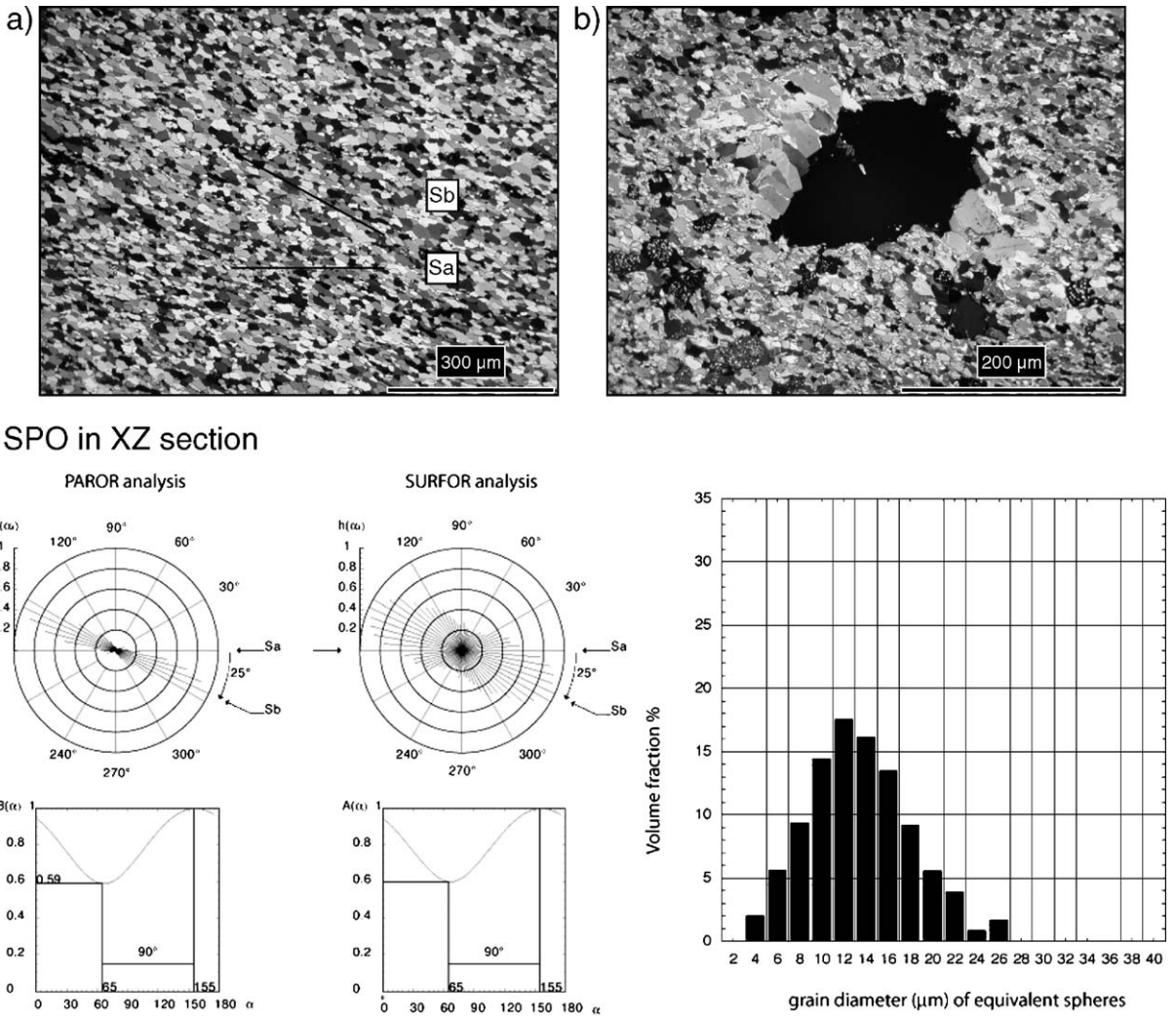

Fig. 14. Microstructure of sample Sa1a4 from locality 2. a, b) Photomicrographs of thin sections in cross-polarised light. Oblique grain shape preferred orientation and asymmetric calcite pressure fringes developed at the rim of detrital quartz grain are both indicative of sinistral shear. c) Microstructural analysis. Grain shape preferred orientation is oblique to Sa by 25° compatible with sinistral shearing of the rock. Grain size distribution is similar to that in *XZ* sections of samples MPY2 and MPY28.

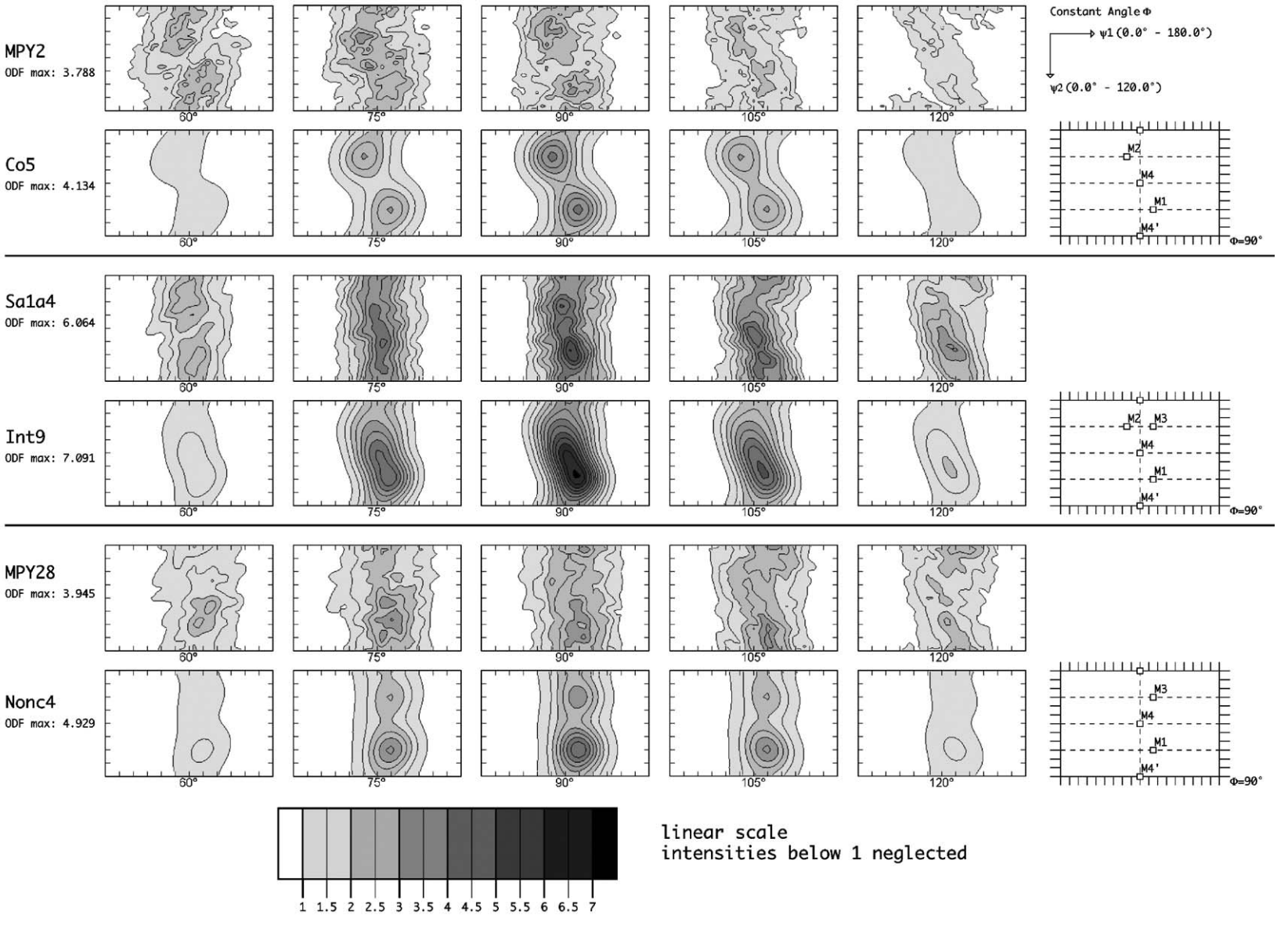

Fig. 15. ODF sections for constant Φ between 60° and 120° for the three most recrystallised samples (MPY2 from profile 1, Sa1a4 from locality 2, MPY28 from profile 2) and for three corresponding idealized model distributions (co5, int9 and nonco4). The ideal crystal orientations M1, M2, M3, M4, M4′ at Φ=90° are illustrated in Fig 16.

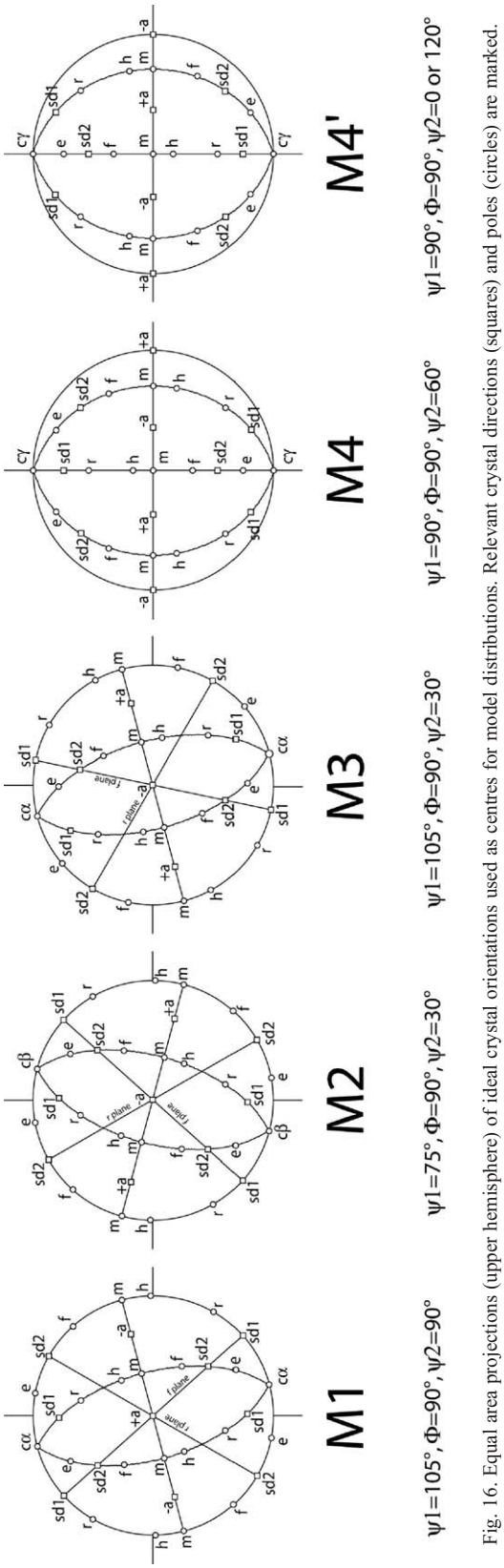

Fig. 16. Equal area projections (upper hemisphere) of ideal crystal orientations used as centres for model distributions. Relevant crystal directions (squares) and poles (circles) are marked.

inclined at 60° from it. The *c*-axis is tilted by 15° in the sense of shear, which is confirmed by the CIP pole figure (Fig. 9b).

Both microstructure and texture of the dynamically recrystallised matrix indicate a monoclinic symmetry, with the structural *Y*-direction as the two-fold symmetry axis.

4.4. SEM analysis of samples MPY2 and MPY28

The content in second phase particles of samples MPY2 (orthorhombic microfabric) and MPY28 (monoclinic microfabric) was analysed. Samples were prepared according to the two-step etching technique described by Herwegh (2000) and observed under a scanning electron microscope in backscattered electron mode (Fig. 13). Quartz and micas inclusions are distinguished on the basis of their shape and backscatter contrast. No systematic differences in density, size and distribution of second phase particles have been observed between samples MPY2 and MPY28.

4.5. Ultramylonite sample with asymmetric characteristics

Sample Sa1a4 was taken at locality 2 (Fig. 2), which is east of and along-strike from the outcrop of the two profiles at locality 1. It originates from the hinge of a fold that re-deformed previously formed calcite mylonites and separates two basement boudins including their Eocene cover. The grain size distribution is very similar to those found in samples MPY2 and MPY28, and likewise the dynamically recrystallised matrix covers more than 90% of the volume. The microstructure shows a clear grain shape foliation Sb oriented at 25° to the foliation (Fig. 14a). The grains show sharp extinction and no deformation twinning. Incipient S–C type structures are locally recognizable. Calcite pressure shadows at the rims of detrital quartz grains show an asymmetry and confirm a sinistral sense of shearing (Fig. 14b). Quantitative analysis (Fig. 14c) on the *X*–*Z* section yields an average aspect ratio of 0.59 with preferred elongation at 25° to the lineation, and a grain size mode of about 12 μm.

This sample Sa1a4 shows a texture that is intermediate between that of samples MPY2 and MPY28 (Fig. 12, bottom): The *c*-axes form a broad and strong maximum roughly normal to the foliation. The *r* planes and the *a* directions are similarly oriented as in MPY28, whereas *sd1* and *sd2* are similar to the patterns in MPY2. The symmetry of the pole figures deviates visibly from monoclinic about the *Y*-axis of the actually inferred

Table 1
Volume fractions of orientation components in the three model distributions

Texture components [%]	Random	M1	M2	M3	M4	M4′
Model						
Co5	75	10	10	0	2.5	2.5
Int9	50	17.5	7.5	5	15	5
Nonco4	75	12.5	0	7.5	2.5	2.5

structural reference frame, but could be brought into approximate orthorhombic symmetry, if the reference axes *X* and *Y* would have been rotated within the foliation plane by 30°.

4.6. ODF sections and ideal crystal orientation models

In the following, the different texture types found in profiles 1 and 2 and at locality 2 will be discussed. Samples MPY2 and MPY28 are used to represent profiles 1 and 2, respectively, since they exhibit the most strongly developed textures in the two series of samples. Sample Sa1a4 from locality 2 represents a third texture type found repeatedly along the RYSZ.

All textures observed for the limestone mylonites have in common that the *c*-axes are preferentially oriented towards directions at the pole figure periphery and nearly normal to the foliation plane. Consequently, the ODF sections displayed in Fig. 15 are restricted to sections between $\Phi=60°$ and 120°, where the highest ODF densities occur along fibres for fixed Euler angles close to $\Phi=90°$ and $\psi_1=90°$ and variable ψ_2.

Apart from this general similarity, the three sample textures occupy several orientations with different frequency. In an attempt to highlight these differences, model textures are constructed from a set of five ideal crystal orientation components M1, M2, M3, M4 and M4′. The orientations (defined in Fig. 16) and width (40°) of the components were fixed, and only their volume fraction, i.e. their relative weight, was varied, until a satisfying match to the sample textures was found by manual trial-and-error (Table 1). It is emphasized that all three model textures contain between 50 and 75% volume of grains with orientations drawn from a uniform distribution, which means that the visible ODF maxima are actually built of comparatively small volume portions of the sample. In all three cases, M1 is the strongest component, while the second strongest component is either M2 (profile 1) or M3 (profile 2) or M4 (locality 2).

Orientation M1 places the *c*-axis at an angle of 15° counter clockwise from the *Z*-direction of the sample. Two single poles of *r* and *f* planes are located at the periphery of the pole figure at angles of about 60° and 50° from *Z* in a conjugate geometry, respectively. These *r* and *f* planes contain one of the *sd2* or one of the *sd1* directions at the periphery of the pole figure. A second *sd2* direction in the *f* plane is not far off the periphery of the pole figure.

Orientation M2 results from M1 by a rotation of 180° around either the *X* or *Z*-axis. Its projection looks like

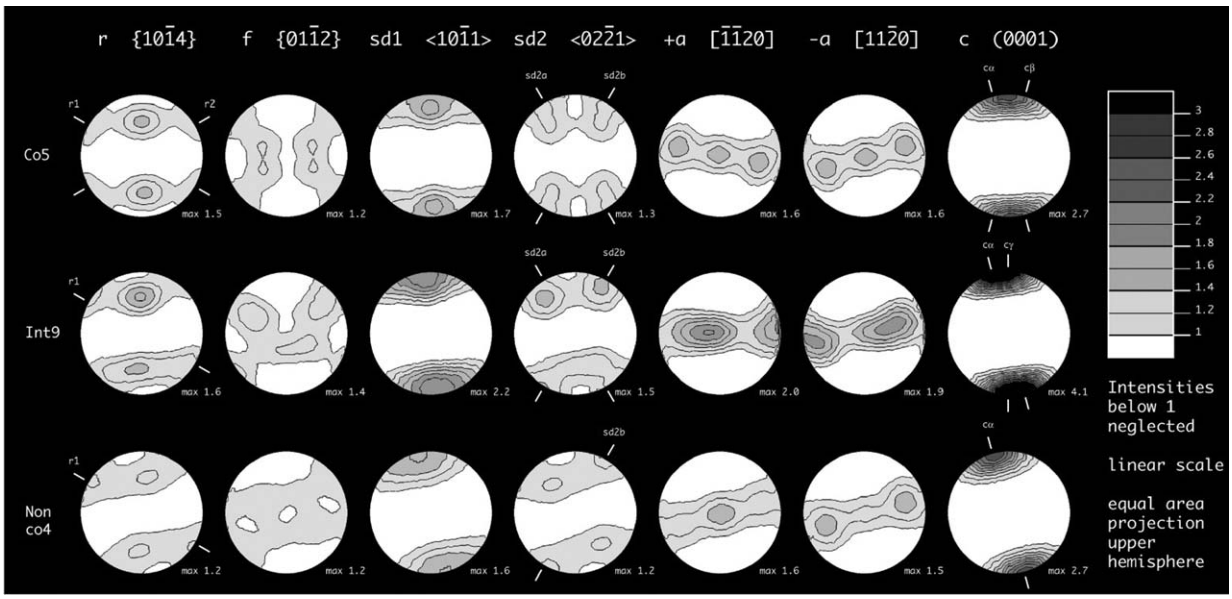

Fig. 17. Pole figures for the three idealized model distributions (co5, int9 and nonco4); same cases as in Fig. 15. Same representation as for the studied samples (Figs. 8 and 12).

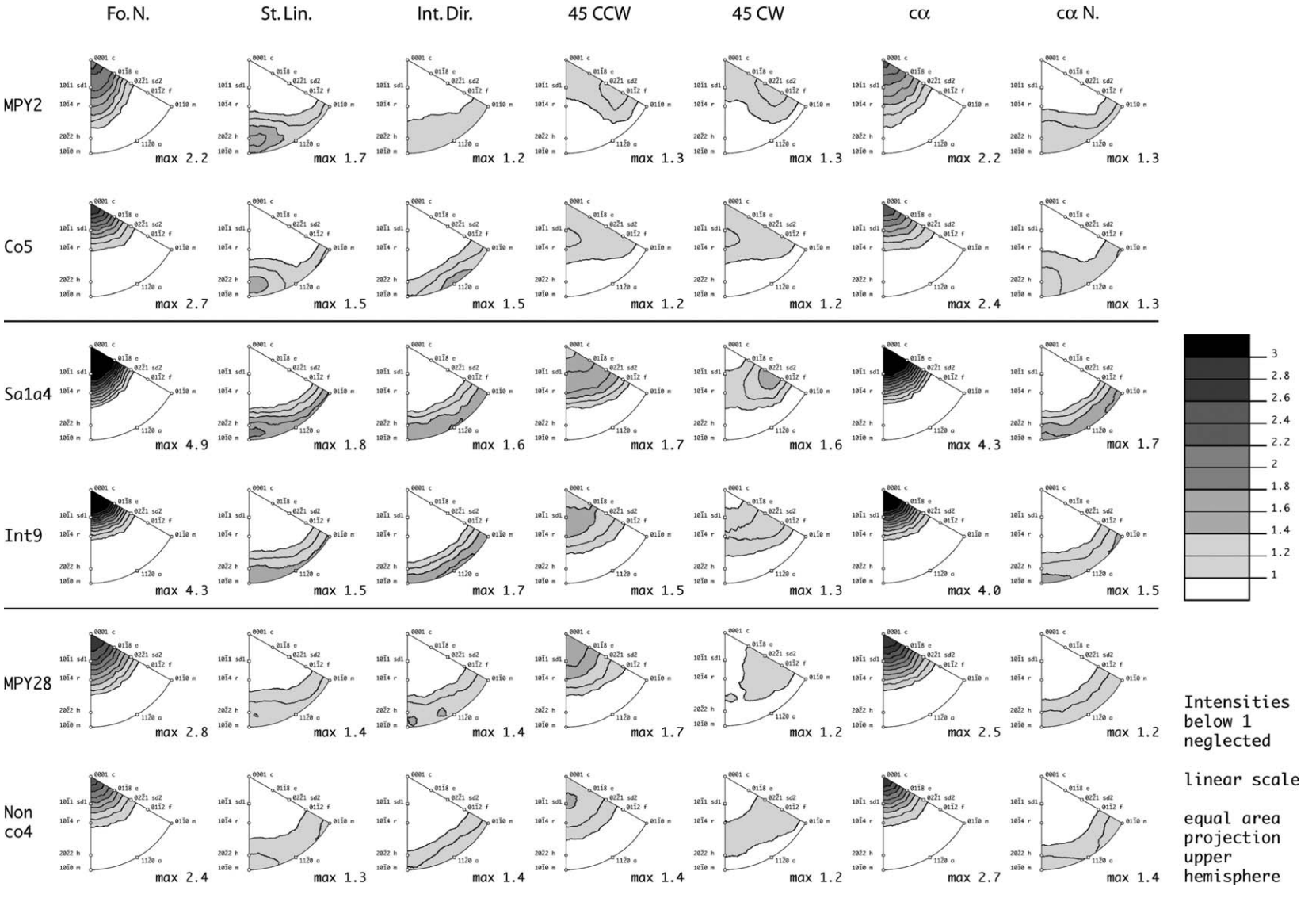

Fig. 18. Inverse pole figures for the three most recrystallised samples (MPY2 from profile 1, Sa1a4 from locality 2, MPY28 from profile 2) and for three idealized model distributions (co5, int9 and nonco4), same cases as in Fig. 15. Sample reference directions are foliation normal (Fo. N.), stretching lineation (St. Lin.), intermediate direction (Int. Dir.), two conjugate directions at 45° between lineation and foliation normal, the directions of *c*-axis maxima (cα and cβ) and perpendicular to them (cαN and cβN) along the pole figure periphery. Contouring as in Fig. 8, equal area projection of upper hemisphere.

the mirror image of M1 with respect to either the *Y*–*Z* or *X*–*Y* plane, but with the sign of the *a*-axes inverted.

Orientation M3 is related to M1 by a 60° rotation around the *c*-axis at cα. Both orientations place the basal plane at an angle of 15° counter clockwise from the plane normal to *Z* (foliation). Their projections appear as mirror positions with respect to the basal plane, again with sign inversion for the *a*-axes.

The orientations M1, M2 and M3 have a two-fold symmetry axis (crystal *a*-axis) parallel to *Y*. Thus a texture that only consists of any amount of these components has at least monoclinic symmetry with symmetry axis *Y*. A texture only with M1 and M2 in equally large portions possesses orthorhombic sample symmetry. If only M1 and M3 would be present in equal shares, then the texture would resemble hexagonal crystal (and sample) symmetry with respect to the crystal *c*- and *a*-axes.

The orientations M4 and M4′ have their *c*-axis parallel to *Z*, and one of the *a*-axes parallel to *X*. They are mutually related by a 180° rotation around *Y*. If they are equally present then the texture preserves monoclinic symmetry, otherwise the two-fold symmetry around *Y* is broken.

The pole figures for the three models are shown in Fig. 17 to be compared with those for the samples of profile 1 (Fig. 8), profile 2 (Fig. 12) or locality 2 (Fig. 12, bottom). They resemble particularly the symmetry of the three texture types, which is orthorhombic for profile 1 (model co5), monoclinic for profile 2 (model nonco4), and asymmetric for locality 2 (model int9).

4.7. Inverse pole figures

Inverse pole figures (IPF) were calculated in order to show the preferential orientation of crystal planes and directions with respect to certain sample directions (Fig. 18). These are foliation normal (*Z*=FoN), stretching lineation (*X*=StLin), intermediate direction (*Y*=IntDir), two conjugate directions at 45° between *X* and *Z* (45° CCW and 45° CW), directions 15° counter clockwise (cα) and 75° clockwise (cαN) from *Z* around *Y*, directions 15° clockwise (cβ) and 75° counter clockwise (cβN) from *Z* around *Y*.

Like the ODF and pole figures, the IPF show similar general characteristics. The IPF for *Z* and cα have the sharpest concentrations, which are towards the *c*-axis. The IPF for *X* and *Y* show girdle distributions along directions in the basal planes, where the lineation (and similarly cαN) is preferentially aligned normal to poles of *m*-prisms or *h*-rhombohedra, and the intermediate direction has a somewhat higher concentration of *a*-axes. The IPF for the two conjugate directions (45° CCW, 45° CW) show maxima near *r* and *f* rhombohedral planes and *sd1* and *sd2* directions. Subtle differences are noticed, as only samples from profile 1 and from locality 2 show some shoulder towards *r* in the IPF for *Z*, and only for profile 1 the two IPF for 45° CCW and 45° CW are identical, as expected for symmetry reasons.

5. Discussion

5.1. Deformation mechanisms

The microfabric evolution shows the following characteristics with increasing distance to the basement along both profiles 1 and 2: (1) the extent of dynamic recrystallisation increases, (2) the dynamically recrystallised grains show an increasing degree of shape preferred orientation, and (3) increasingly stronger textures develop. These observations lead to the interpretation that the spatial gradient across the profiles also maps gradients in finite strain, and that deformation has most likely occurred by dominant dislocation creep accompanied by dynamic recrystallisation. While there is some evidence also for pressure solution and re-precipitation, grain boundary sliding and/or diffusion creep were presumably not the dominant deformation mechanisms in our samples, because those are expected to result in rocks with isotropic fabrics (Edington et al., 1976; Schmid et al., 1977; Padmanabhan and Davies, 1980; Schmid et al., 1987; Rutter and Brodie, 1988).

5.2. Kinematics of deformation: coaxial vs. non-coaxial

The samples from profile 1 exhibit microfabric characteristics, notably in terms of SPO and texture measurements, which possess orthorhombic sample symmetry with respect to the structural reference frame, defined by lineation *X*, foliation normal *Z* and intermediate strain axis *Y*. Fabrics are approximately symmetric with respect to rotations by 180° around these three axes, which is almost equivalent to mirror symmetries perpendicular to them. They do not indicate any preferred sense of shearing, i.e. do not contain any record of dominant non-coaxial (simple shear) deformation. We interpret these rocks to be deformed on a coaxial deformation path, where all three principal axes are distinct, which is presumably close to plane strain, i.e. pure shear. The inferred principal stress axes nearly coincide with the axes of the structural reference frame of profile 1, i.e. σ1 is oriented about normal to the macroscopic foliation and σ3 falls near the stretching lineation, which independently demonstrates conditions of coaxial strain.

The samples from profile 2 possess microstructures and textures that have no more than monoclinic sample symmetry with a single two-fold symmetry axis around the intermediate strain axis *Y*. It is emphasized that the fabric symmetry could not be raised just by redefinition of the reference frame, but that there are distinct features oriented relative to each other that break orthorhombic symmetry. These are S–C fabrics and asymmetric pressure fringes in the microstructures, and the position and weight of orientation components relative to each other as well as relative to primary and secondary foliation planes in the textures. Only the intermediate axes σ2 of the inferred principal stress tensor roughly coincides with an axis (the *Y*-axis) of the structural reference frame of profile 2, while σ1 and σ3 are oriented at equally large angles to foliation and lineation. These observations are taken as evidence that deformation of these samples must have occurred on a non-coaxial deformation path with vorticity axis towards *Y*, i.e. simple shear in the idealized case of plane strain deformation.

In summary, the samples from the two profiles exhibit contrasting types of fabrics on a microscopic scale. The microstructural data independently confirms the conclusions made for the macroscopic scale (Fig. 3). All data suggest that the specimens of profiles 1 and 2, i.e. specimens with identical lithological compositions and strained under the same P–T conditions, deformed in contrasting kinematic regimes. As the deformation mechanisms have been identical, and since the influence of second phase particles has been ruled out in Section 4.4 we interpret the differences in texture as due to the different kinematics of deformation.

5.3. Asymmetric fabrics

The microstructure of sample Sa1a4 indicates that this rock was deformed by a significant amount of rotational deformation. Its texture shows similarities with the textures of sample MPY2 (profile 1, coaxial) as well as of sample MPY28 (profile 2, non-coaxial). It differs from both as it does not equally balance the orientation components around M4 and M4′. This means that none of the three structural reference axes is actually a two-fold symmetry axis anymore, and the strain path must have deviated from plane strain. It remains puzzling that the texture resembles nearly orthorhombic symmetry with respect to axes rotated by about 30° around *Z*, i.e. shifting *X* and *Y* within the foliation plane, because those apparent symmetry directions have no pendant in the field when back-projected into geographic coordinates.

5.4. Suitably oriented slip systems

The following slip systems have been confirmed as dominant slip systems for calcite in experiments of Turner et al. (1954), Griggs et al. (1960), Turner and Heard (1965), Weiss and Turner (1972), Braillon (1976), Spiers and Wenk (1980), and De Bresser and Spiers (1990, 1993, 1997):

r {10–14} *sd2* <02–21>	Turner et al., 1954
	Griggs et al., 1960
	Turner and Heard, 1965
	Weiss and Turner, 1972
	Braillon, 1976
	Spiers and Wenk, 1980
	De Bresser and Spiers, 1990
	De Bresser and Spiers, 1993
f {01–12} *sd2* <02–21>	Turner et al., 1954
	Griggs et al., 1960
	Spiers and Wenk, 1980
f {01–12} *sd1* <10–11>	De Bresser and Spiers, 1990
	De Bresser and Spiers, 1993
	De Bresser and Spiers, 1997
c {0001} <*a*>	De Bresser and Spiers, 1997

Assuming ideal plastic rheology of an isotropic material, the maximum shear stress is resolved on two conjugate planes oriented at 45° between the two extreme principal stress directions, where the normal to one plane is also the shear direction on the other plane. In coaxial deformation, the principal directions of stress fall together with those of strain rate as well as finite strain, thus the maximum shear stress is expected on planes at 45° to *X* and *Z*. In simple shear as a special case of non-coaxial deformation, the principal directions are identical for stress and strain rate, but those of finite strain rotate with progressive deformation around the *Y*-axis and converge to a position, where σ1 and σ3 make equal angles of 45° both to *X* and *Z*. Given that deformation was dominated by simple shearing and has reached large shear strain, the angle between the shear zone boundary and the macroscopic foliation is very small, and it can be assumed that the σ1 direction lies for sinistral shear near the upper-right/lower-left corners of the *XZ*-plane. In other words, the maximum shear stress is then resolved on the foliation plane and on the plane perpendicular to the lineation. While both positions are equally suited at a local scale, only shear on the foliation plane along lineation is geometrically feasible at the larger scale of a shear zone.

For any given crystal orientation, those slip systems are most likely to be activated on which the highest shear stress is resolved, i.e. which are closest to the above planes and directions of maximum resolved shear stress. Our paleostress analysis may have given some

indications for the principal directions of stress, but there is hardly any constraint on the magnitudes of the principal stresses. Therefore we restrict the following discussion on qualitative arguments instead of attempting to quantify the resolved shear stress by means of the Schmidt factor, which would require further assumptions on the complete stress tensor.

For coaxial deformation (e.g. pure shear) as inferred for the samples from profile 1, their ideal crystal orientations M1 and M2 (Figs. 14 and 15) both have a *r*[*sd2*] and a *f*[*sd1*] slip system suitably oriented, and to a lesser extent also a *f*[*sd2*] system (Fig. 15). The *a* direction that is parallel to the *Y*-axis is geometrically disabled to slip, and the other two basal[*a*] slip systems are rather unsuitably oriented. For the orientations M4 and M4′ (Figs. 14 and 15), the resolved shear stress vanishes for all three basal slip systems, but slip on conjugate pairs of *r*[*sd2*] and *f*[*sd2*] is possible.

For non-coaxial deformation (e.g. simple shear) as inferred for the samples from profile 2, their main orientations M1 and M3 have *r* and *f* planes oriented at 60° and 50° to the foliation, which thus are not well oriented slip planes. The basal plane, inclined at 15° to the foliation "with the sense of shear", is the only potential slip plane that is close to the orientation of the bulk shear plane, and which could have been activated by duplex slip along the two *a*-directions that are not parallel to *Y*. However, given the angle of 15° between basal plane and foliation, it appears that antithetic slip along the *f* or *r* planes would also be needed in order to maintain homogeneous simple shear deformation (Mancktelow, 1987; Schmid, 1994). Basal [*a*]-slip systems are perfectly oriented for the orientations M4 and M4′, which, however, do not constitute the primary orientation components in the textures along profile 2.

5.5. Textures in experimentally deformed samples

The pure shear textures are similar to the "high temperature type" textures obtained in pure shear experiments of micritic limestones performed by Wagner et al. (1982) in a testing apparatus with three independent stress actuators at 400 °C. This experimentally produced texture consists of two stronger maxima at the periphery of the pole figure, 30° on either side of the σ1 direction and a third weaker maximum parallel to the σ3 direction. Our textures from profile 1 somewhat resemble the HT-type textures of Wagner et al. (1982), as far as both show orthorhombic texture symmetry with double *c*-axis maxima in the *X*–*Z* plane closer to *Z* than to *X*. Slip on the *r* and *f* planes was inferred to be the dominant deformation mechanism. The corresponding microstructures (Kern and Wenk, 1983) show a strong SPO consistent with the imposed coaxial strain path and no twinning or dynamic recrystallisation. Twinning is also not observed in the case of our natural samples at Rocher de l'Yret. Hence the absence of twinning at higher temperatures appears to be an important criterion of distinction between "low" and "high temperature" deformation in the sense of Wagner et al. (1982), especially in the texture evolution (see also Schmid et al., 1987 their "twinning" vs. their "intracrystalline slip" regime). Twinning activity is further suppressed due to the small grain size in the limestone and in our mylonites, while a coarse grained marble would still easily twin under the same conditions. Model simulations of the texture evolution by dislocation glide are consistent with the observed textures in the absence of twinning (Wagner et al., 1982; Kern and Wenk, 1983; Wenk et al., 1987).

Since these pure shear experiments have not been carried out to large enough strains the role of dynamic recrystallisation for texture evolution could not be assessed experimentally. It is likely that recrystallisation by subgrain rotation and local boundary migration processes do not alter the texture type but strengthen the texture with progressive deformation similarly as observed in the RYSZ samples of profile 1.

None of the studies of texture evolution in experimental simple shear (Schmid et al., 1987; Pieri et al., 2001a,b) have produced exactly the same textures as those observed in the RYSZ. Schmid et al. (1987) observed similar textures in their 800 °C "grain boundary migration regime" experiments with a distinct *c*-axis maximum rotated with the sense of shear relative to foliation, which they also inferred due to a dominating contribution of slip in the basal plane. Preferred orientations similar to M3 with *c*-axes inclined with the sense of shear developed in torsion experiments of Carrara marble at 500 °C and 600 °C after very large shear strain ($\gamma \geq 10$, Barnhoorn et al., 2004). Twinning of the initially coarse grained marble controlled the texture formation at small strain and caused a *c*-axis maximum opposite to the sense of shear. Twinning was less important in the fine grained mylonite at large strain, which then caused the texture transition.

5.6. Texture evolution in naturally deformed limestones

One geometric assumption often made for texture interpretation is that during progressive simple shear deformation accompanied by dynamic recrystallisation, one or several distinct slip planes tend to align parallel or at small angles to the bulk shear plane and corresponding slip directions tend to align with the bulk shear direction of the rock (Nicolas, 1976; Etchecopar, 1977; Bouchez,

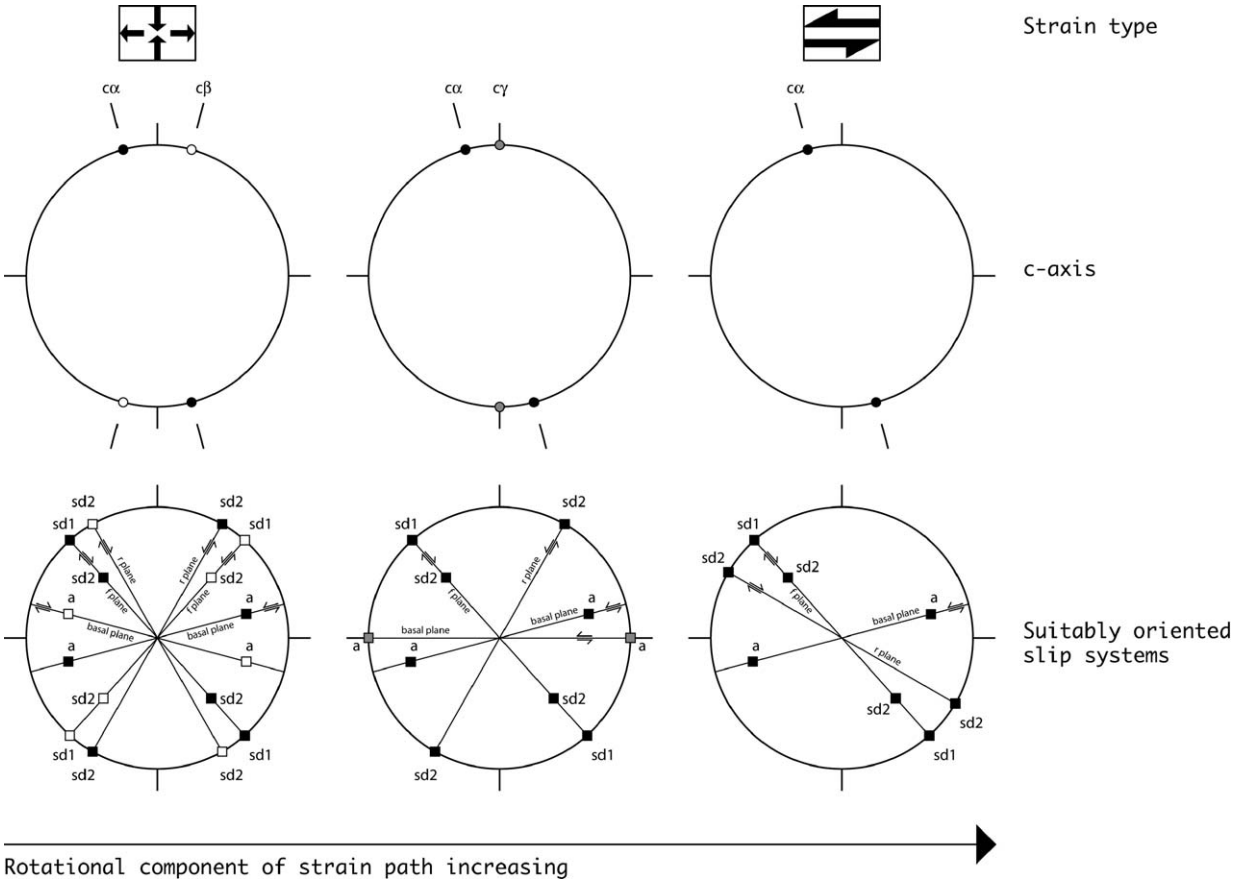

Fig. 19. Sketch summarizing the evolution of the calcite *c*-axis distribution during the transition from coaxial dominated to non-coaxial dominated deformation under conditions suppressing twinning. Poles and projections of slip planes and slip directions are reported for the main ideal orientation components, which are suitably oriented for slip under the assumed kinematics. Black symbols belong to orientations with *c*-axis at cα (M1, M3), white symbols at cβ (M2), grey symbols at cγ (M4, M4′).

1978; Schmid, 1994). Such an orientation of certain slip systems aligns the microscopic deformation scale (simple shear by crystal plastic slip on one slip system) with that of the macroscopic deformation. This alignment is only possible for simple shear kinematics.

The previous discussion points out that there seems to be a gradual shift from predominant rhomb slip (*r* and *f* slip) in pure shear to predominant basal slip in simple shear. This shift would imply that the kinematics of deformation has an influence on the activity of the slip systems. At first sight this appears intriguing, as the critical resolved shear stresses of the various slip systems should not depend on the kinematics of deformation. However, the texture evolution is also influenced by dynamic recrystallisation (Schmid, 1994; Wenk and Tome, 1999). In the case of simple shear, grains with their *c*-axis orientations inclined against the sense of shear are unsuitably oriented for basal slip and may hence be eliminated by nucleation and preferential growth of grains that are suitably oriented in terms of basal slip. Provided that grains with orientations that are not suitably oriented for basal slip act as local stress raisers during simple shearing, they could preferentially be consumed by dynamic recrystallisation. Dynamic recrystallisation results in a stationary cycle of newly formed small grains (through subgrain rotation and/or bulging), which grow and deform by slip until they will be consumed again by their neighbours. While individual grains permanently change their size, shape and orientation, the microstructure and texture on average remain constant with strain after a certain initialisation. The rate of these recrystallisation cycles is largely affected by the impurity content at the micro- and nanoscale (Herwegh and Kunze, 2002). The nummulitic limestone of RYSZ must be considered a rather impure calcite rock in that sense, as it contains enough impurities to prevent grain growth and to decelerate the microstructural resetting.

In summary of our empirical observations, a texture transition as function of strain path is schematically

depicted in Fig. 19, following ideas proposed for quartz by Schmid and Casey (1986). We emphasize, however, that in case of calcite the simple-shear end-member does not involve slip along one single slip system only, namely the basal plane, but antithetical slip on *r* and *f* also contributed to deformation. Slip along a single slip system is only possible if this slip system is perfectly aligned with the shear zone boundary and no incompatibilities arise at grain boundaries. The obliquity between basal plane and foliation is too high (15°) in case of the ultramylonites, for which the foliation is expected to nearly coincide with the shear zone boundary.

To our knowledge most published oblique calcite *c*-axis textures (see for example Behrmann, 1983; Dietrich and Song, 1984; Schmid et al., 1987; Ratschbacher et al., 1991) exhibit maxima oriented "against the sense of shear", as expected when calcite *e*-twinning is responsible for texture evolution (Schmid et al., 1987). In our samples, however, twinning was suppressed by the small grain size and elevated temperatures. The *c*-axis maxima oriented "with the sense of shear" correspond to what is consistently found for quartz mylonites (Lister and Price, 1978; Bouchez and Pecher, 1981; Malavieille and Etchecopar, 1981; Schmid and Casey, 1986; Bhattacharya and Weber, 2004), which are similarly attributed to dominant basal slip.

Two conditions need to be satisfied if the interpretation of the texture transition discussed so far is correct: (1) the slip systems involved (*r*, *f* and basal plane) need to have comparable critical resolved shear stresses at the temperature conditions of deformation, and (2) there must be very subordinate twinning during deformation. Condition (1) appears to be satisfied for the high temperature deformation regime (De Bresser and Spiers, 1997). Condition (2) appears to be satisfied in many experimentally and naturally deformed samples where dynamic recrystallisation dominates (Wagner et al., 1982; Schmid et al., 1987; Lafrance et al., 1994; Pieri et al., 2001a,b).

Whether calcite textures and their asymmetry can be used as unequivocal shear sense criteria remains an issue of further research and microstructural criteria such as oblique SPO are certainly more reliable criteria. If no twinning occurs, it appears that *c*-axis maxima are either normal to foliation or rotated synthetically with the sense of shear. If twinning is dominant during deformation, the *c*-axis maximum will be rotated antithetically to, i.e. "against" the shear sense. Then an asymmetry opposite to that observed for the samples from Rocher de l'Yret would be expected. Thus, for all practical purposes, calcite textures should only be used in conjunction with shape fabric analyses and microstructural studies of twinning and dynamic recrystallisation.

6. Summary and conclusions

Two sample series from the Rocher de l'Yret shear zone were studied, which deformed at the same time under conditions of low anchizone metamorphic conditions. From the fabric analysis of both zones it is concluded that orthorhombic SPO symmetry is indicative of pure shear dominated deformation while monoclinic SPO symmetry is indicative of simple shear dominated deformation. The textures of these samples also show orthorhombic and monoclinic symmetries, respectively, and confirm the conclusion that the two profiles represent cases that are close to the pure and simple shear end members.

In general, the SPO and texture analysis of samples from the Rocher de l'Yret deformation zone indicates that the symmetry of calcite fabrics appears to indicate simple shear deformation for monoclinic fabrics. Orthorhombic fabric symmetry, however, may but does not necessarily has to indicate pure shear deformation, because the latter may also be produced by simple shear strain paths as documented in the literature (Schmid et al., 1987; Lafrance et al., 1994; Pieri et al., 2001a,b). The type of *c*-axis patterns observed in the simple shear samples shows some deviation from textures reported from other naturally deformed calcitic rocks, where an oblique *c*-axis maximum typically occurs opposite to the sense of shear due to *e*-twinning. A *c*-axis maximum rotated synthetically with the sense of shear may be also used as a shear sense indicator provided that it can be demonstrated that twinning in calcite was of subordinate importance compared to basal slip, which is often the case for fine grained calcite mylonites.

7. Software used

[1] Tectonic VB 1.5a Ortner, H., 2001. http://geopal.uibk.ac.at/tvb/front.html.
[2] NIH image public domain software http://rsb.info.nih.gov/nih-image/download.html.
[3] Stripstar http://www.unibas.ch/earth/micro/software/grainsize/grainsize.html.
[4] MENTEX Schaeben et al., 1990.
[5] BEARTEX Wenk et al., 1998.

Acknowledgement

The authors wish to thank all colleagues from the tectonics group at Basel University for stimulating discussions, Pierre Dèzes for assistance in computer

programming, Willy Tschudin for preparing excellent ultrathin sections. Thorough reviews by Marco Herwegh, Bernd Leiss and a third anonymous reviewer significantly improved the manuscript. This study was funded by the Swiss National Science Foundation.

References

Angelier, J., Mechler, P., 1977. Sur une methode graphique de recherche des contraintes principales egalement utilisables en tectonique et en seismologie: la methode des diedres droits. Bulletin de la Societe Geologique de France 19 (6), 1309–1318.

Aprahamian, J., 1974. La cristallinite de l'illite et les mineraux argileux en bordure des massifs cristallins externes de Belledonne et du Pelvoux (variations et relations possibles avec des evenements tectoniques et metamorphiques alpins). Geologie Alpine 50, 5–15.

Aprahamian, J., 1988. Cartographie du metamorphisme faible a tres faible dans les Alpes francaises externes par l'utilisation de la cristallinite de l'illite. Geodinamica Acta 2 (1), 25–32.

Bagnoud, A., Wernli, R., Sartori, M., 1998. Decouverte de foraminiferes planctoniques paleogenes dans la zone de Sion-Courmayeur a Sion (Valais, Suisse). Eclogae Geologicae Helvetiae 91 (3), 421–429.

Barnhoorn, A., Bystrichy, M., Burlini, L., Kunze, K., 2004. The role of recrystallisation on the deformation behaviour of calcite rocks: large strain torsion experiments on Carrara marble. Journal of Structural Geology 26 (5), 885–903.

Beach, A., 1981. Thrust structures in the eastern Dauphinois Zone (French Alps), north of the Pelvoux Massif. Journal of Structural Geology 3 (3), 299–308.

Behrmann, J.H., 1983. Microstructure and fabric transitions in calcite tectonites from the Sierra Alhamilla (Spain). Geologische Rundschau 72 (2), 605–618.

Bestmann, M., Kunze, K., Matthews, A., 2000. Evolution of a calcite marble shear zone complex on Thassos Island, Greece; microstructural and textural fabrics and their kinematic significance. Journal of Structural Geology 22 (11–12), 1789–1807.

Bhattacharya, A.R., Weber, K., 2004. Fabric development during shear deformation in the Main Central Thrust Zone, NW-Himalaya, India. Tectonophysics 387, 23–46.

Bouchez, J.L., 1978. Preferred orientations of quartz <a> axes in some tectonites; kinematic inferences. Tectonophysics 49 (1–2), T25–T30.

Bouchez, J.L., Pecher, A., 1981. The Himalayan Main Central Thrust pile and its quartz-rich tectonites in central Nepal. Tectonophysics 78 (1–4), 23–50.

Braillon, P.A.S.J., 1976. Deformation plastique de monocristaux de calcite en compression suivant <001>. Physica Status Solidi. A, Applied Research 36, 637–646.

Bunge, H.J., 1982. Texture Analysis in Material Science — Mathematical Methods. Butterworth, London.

Bürgisser, J., Ford, M., 1998. Overthrust shear deformation of a foreland basin; structural studies south-east of the Pelvoux Massif, SE France. Journal of Structural Geology 20 (11), 1455–1475.

Burlini, L., Marquer, D., Challandes, N., Mazzola, S., Zangarini, N., 1998. Seismic properties of highly strained marbles from the Splügenpass, central Alps. Journal of Structural Geology 20, 277–292.

Butler, R.W.H., 1992. Thrust zone kinematics in a basement-cover imbricate stack; eastern Pelvoux Massif, French Alps. Journal of Structural Geology 14 (1), 29–40.

Casey, M., 1981. Numerical analysis of X-ray texture data; an implementation in Fortran allowing triclinic or axial specimen symmetry and most crystal symmetries. Tectonophysics 78 (1–4), 51–64.

Casey, M., Kunze, K., Olgaard, D.L., 1998. Texture of Solnhofen Limestone deformed to high strains in torsion. Journal of Structural Geology 20 (2–3), 255–267.

Ceriani, S., Fuegenschuh, B., Schmid, S.M., 2001. Multi-stage thrusting at the "Penninic Front" in the Western Alps between Mont Blanc and Pelvoux massifs. International Journal of Earth Sciences 90 (3), 685–702.

De Bresser, J.H.P., 1989. Calcite *c*-axis textures along the Gavarnie thrust zone, central Pyrenees. Geologie en Mijnbouw 68, 367–375.

De Bresser, J.H.P., Spiers, C.J., 1990. High-temperature deformation of calcite single crystals by r (super+) and f (super+) slip. Geological Society Special Publications 54, 285–298.

De Bresser, J.H.P., Spiers, C.J., 1993. Slip systems in calcite single crystals deformed at 300–800 degrees C. Journal of Geophysical Research 98 (4), 6397–6409.

De Bresser, J.H.P., Spiers, C.J., 1997. Strength characteristics of the r, f, and c slip systems in calcite. Tectonophysics 272 (1), 1–23.

Dietrich, D., Song, H., 1984. Calcite fabrics in a natural shear environment, the Helvetic nappes of western Switzerland. Journal of Structural Geology 6 (1–2), 19–32.

Edington, J.W., Melton, K.N., Cutler, C.P., 1976. Superplasticity. Progress in Materials Science 21, 61–170.

Erskine, B.G., Heidelbach, F., Wenk, H.R., 1993. Lattice preferred orientations and microstructures of deformed Cordilleran marbles; correlation of shear indicators and determination of strain path. Journal of Structural Geology 15 (9–10), 1189–1205.

Etchecopar, A., 1977. A plane kinematic model of progressive deformation in a polycrystalline aggregate. Tectonophysics 39 (1–3), 121–139.

Ford, M., 1996. Kinematics and geometry of early Alpine, basement-involved folds, SW Pelvoux Massif, SE France. Eclogae Geologicae Helvetiae 89 (1), 269–295.

Froitzheim, N., Schmid, S.M., Frey, M., 1996. Mesozoic paleogeography and the timing of eclogite-facies metamorphism in the Alps; a working hypothesis. Eclogae Geologicae Helvetiae 89 (1), 81–110.

Fuegenschuh, B., Schmid, S.M., 2003. Late stages of deformation and exhumation of an orogen constrained by fission-track data; a case study in the Western Alps. Geological Society of America Bulletin 115 (11), 1425–1440.

Gidon, P., 1954. Les rapports des terrains cristallins et de leur couverture sedimentaire, dans les regions orientale et meridionale du massif du Pelvoux. Travaux du Laboratoire de Geologie de la Faculte des Sciences de Grenoble 31, 1–199.

Gidon, M., 1979. Le role des etapes successives de deformation dans la tectonique alpine du massif du Pelvoux (Alpes occidentales). Comptes Rendus Hebdomadaires des Seances de l'Academie des Sciences. Serie D, Sciences Naturelles 288 (9), 803–806.

Gignoux, M., Moret, L., 1938. Description geologique du bassin superieure de la Durance. Travaux du Laboratoire de Géologie de la Faculté des Sciences de Grenoble 21, 1–295.

Griggs, D.T., Turner, F.J., Heard, H.C., 1960. Deformation of rocks at 500 degrees to 800 degrees C. Geological Society of America 39–104.

Heilbronner, R.P., Pauli, C., 1993. Integrated spatial and orientation analysis of quartz c-axes by computer-aided microscopy. Journal of Structural Geology 15 (3–5), 369–382.

Heilbronner, R.P., Pauli, C., 1994. Orientation and misorientation imaging: integration of microstructural and textural analysis. In: Bunge, H.J., Siegesmund, S., Skrotzki, W., Weber, K. (Eds.),

Texture of Geological Materials. DGM Informationsgesellschaft Verlag, Oberursel, pp. 147–164.
Helming, K., Geier, St., Heinitz, J., Leiss, B., Rauschenbach, B., Schwarzer, R.A., Ullemeyer, K., Wenk, H.-R., 1994. Texture estimates by means of components. Zeitschrift für Metallkunde 85, 545–553.
Herwegh, M., 2000. A new technique to automatically quantify microstructures of fine grained carbonate mylonites; two-step etching combined with SEM imaging and image analysis. Journal of Structural Geology 22 (4), 391–400.
Herwegh, M., Berger, A., 2003. Differences in grain growth of calcite; a field-based modeling approach. Contributions to Mineralogy and Petrology 145 (5), 600–611.
Herwegh, M., Kunze, K., 2002. The influence of nano-scale second-phase particles on deformation of fine grained calcite mylonites. Journal of Structural Geology 24 (9), 1463–1478.
Kern, H., Wenk, H.R., 1983. Calcite texture development in experimentally induced ductile shear zones. Contributions to Mineralogy and Petrology 83 (3–4), 231–236.
Kurz, W., Neubauer, F., Unzog, W., Genser, J., Wang, X., 2000. Microstructural and textural development of calcite marbles during polyphase deformation of Penninic units within the Tauern Window (Eastern Alps). Tectonophysics 316, 327–342.
Lafrance, B., White, J.C., Williams, P.F., 1994. Natural calcite *c*-axis fabrics; an alternate interpretation. Tectonophysics 229 (1–2), 1–18.
Leiss, B., Molli, G., 2003. "High-Temperature" texture in naturally deformed Calcite marble from the Alpi Apuane, Italy. Journal of Structural Geology 25, 649–658.
Leiss, B., Ullemeyer, K., 1999. Texture characterisation of carbonate rocks and some implications for the modeling of physical anisotropies, derived from idealized texture types. Zeitschrift der Deutschen Geologischen Gesellschaft 150 (2), 259–274.
Leiss, B., Weiss, T., 2000. Fabric anisotropy and its influence on physical weathering of different types of Carrara marbles. Journal of Structural Geology 22, 1737–1745.
Leiss, B., Siegesmund, S., Weber, K., 1999. Texture asymmetries as shear sense indicators in naturally deformed mono- and poly-phase carbonate rocks. Textures and Microstructures 33, 61–74.
Lister, G.S., Price, G.P., 1978. Fabric development in a quartz–feldspar mylonite. Tectonophysics 49, 37–78.
Malavieille, J., Etchecopar, A., 1981. Ductile shear deformation of quartzite in an alpine crustal thrust (Ambin massif). Tectonophysics 78, 65–71.
Mancktelow, N.S., 1987. Quartz textures from the Simplon fault zone, Southwest Switzerland and North Italy. Tectonophysics 135 (1–3), 133–153.
Merle, O., Brun, J.P., 1984. The curved translation path of the Parpaillon Nappe (French Alps). Journal of Structural Geology 6 (6), 711–719.
Mosar, J., Stampfli, G.M., Girod, F., 1996. Western Prealpes Medianes Romandes; timing and structure; a review. Eclogae Geologicae Helvetiae 89 (1), 389–425.
Nicolas, A., 1976. Flow in upper-mantle rocks; some geophysical and geodynamic consequences. Tectonophysics 32, 93–106.
Oesterling, N., Heilbronner, R., Stünitz, H., Barnhoorn, A. Molli, G., submitted for publication. Strain dependent variations of microstructure and texture in naturally deformed Carrara marble. Tectonophysics.
Padmanabhan, K.A., Davies, G.J., 1980. Superplasticity. Springer. 312 pp.
Panozzo, R.H., 1983. Two-dimensional analysis of shape-fabric using projections of digitized lines in a plane. Tectonophysics 95 (3–4), 279–294.
Panozzo, R.H., 1984. Two-dimensional strain from the orientation of lines in a plane. Journal of Structural Geology 6 (1–2), 215–221.
Passchier, C.W., Trouw, R.A.J., 1996. Microtectonics. Springer. 289 pp.
Pieri, M., Burlini, L., Kunze, K., Stretton, I., Olgaard, D.L., 2001a. Rheological and microstructural evolution of Carrara Marble with high shear strain; results from high temperature torsion experiments. Journal of Structural Geology 23 (9), 1393–1413.
Pieri, M., Kunze, K., Burlini, L., Stretton, I., Olgaard, D.L., Burg, J.P., Wenk, H.R., 2001b. Texture development of calcite by deformation and dynamic recrystallisation at 1000 K during torsion experiments of marble to large strains. Tectonophysics 330 (1–2), 119–140.
Ratschbacher, L., Wenk, H.R., Sintubin, M., 1991. Calcite textures; examples from nappes with strain-path partitioning. Journal of Structural Geology 13 (4), 369–384.
Rutter, E.H., Brodie, K.H., 1988. The role of tectonic grain size reduction in the rheological stratification of the lithosphere. Geologische Rundschau 77 (1), 295–308.
Schaeben, H., Siemes, H., Hoefler, S., Will, G., 1990. Practical application of entropy optimization in quantitative texture analysis. Geological Society Special Publications 54, 375–381.
Schmid, S.M., 1994. Textures of geological materials: computer model predictions versus empirical interpretations based on rock deformation experiments and field studies. In: Bunge, H.J., Siegesmund, S., Skrotzki, W., Weber, K. (Eds.), Texture of Geological Materials. DGM Informationsgesellschaft Verlag, Oberursel, pp. 279–301.
Schmid, S.M., Casey, M., 1986. Complete fabric analysis of some commonly observed quartz *c*-axis patterns. Geophysical Monograph 36, 263–286.
Schmid, S.M., Boland, J.N., Paterson, M.S., 1977. Superplastic flow in finegrained limestone. Tectonophysics 43 (3–4), 257–291.
Schmid, S.M., Casey, M., Starkey, J., 1981. The microfabric of calcite tectonites from the Helvetic Nappes (Swiss Alps). Geological Society of London Special Publication 9, 151–158.
Schmid, S.M., Panozzo, R., Bauer, S., 1987. Simple shear experiments on calcite rocks; rheology and microfabric. Journal of Structural Geology 9 (5–6), 747–778.
Seward, D., Mancktelow, N.S., 1994. Neogene kinematics of the Central and Western Alps; evidence from fission-track dating. Geology 22 (9), 803–806.
Seward, D., Ford, M., Bürgisser, J., Lickorish, H., Williams, E.A., Meckel, L.D., 1999. Preliminary results of fission-track analyses in the southern Pelvoux area, SE France. In: Gosso, G., Jadoul, F., Sella, M., Spalla, Maria I. (Eds.), 3rd workshop on Alpine Geological Studies. Memorie di Scienze Geologiche, 51(1), pp. 25–31.
Spencer, S., 1992. A kinematic analysis incorporating incremental strain data for the frontal Pennine zones of the western French Alps. Tectonophysics 206 (3–4), 285–305.
Spiers, C.J., Wenk, H.R., 1980. Evidence for slip on r and f in the positive sense in deformed calcite single crystals. American Geophysical Union; 1980 fall meeting. Eos, Transactions 61 (46), 1128.
Tagami, T., Galbraith, R.F., Yamada, R., Laslett, G.M., 1998. Revised annealing kinetics of fission tracks in zircon and geological implications. In: Van den Haute, P., De Corte, F. (Eds.), Advances in Fission-Track Geochronology. Kluwer Academic Publishers, Dordrecht, pp. 99–112.
Trullenque, G., 2005. Tectonic and microfabric studies along the Penninic Front between Pelvoux and Argentera massifs (Western Alps, France). PhD thesis, Basel University, 287 pp.

Turner, F.J., Heard, H.C., 1965. Deformation in calcite crystals at different strain rates. University of California Publications in Geological Sciences 46, 103–126.

Turner, F.J., Griggs, D.T., Heard, H.C., 1954. Experimental deformation of calcite crystals. Geological Society of America Bulletin 65 (9), 883–933.

Wagner, F., Wenk, H.R., Kern, H., Houtte, P.V., Esling, C., 1982. Development of preferred orientation in plane strain deformed limestone; experiment and theory. Contributions to Mineralogy and Petrology 80 (2), 132–139.

Weiss, L.E., Turner, F.J., 1972. Some observations on translation gliding and kinking in experimentally deformed calcite and dolomite, flow and fracture of rocks. Geophysical Monograph 16, 95–107.

Wenk, H.R., Tome, C.N., 1999. Modeling dynamic recrystallisation of olivine aggregates deformed in simple shear. Journal of Geophysical Research, B: Solid Earth and Planets 104 (11), 25,513–25,527.

Wenk, H.R., Takeshita, T., Bechler, E., Erskine, B.G., Matthies, S., 1987. Pure shear and simple shear calcite textures; comparison of experimental, theoretical and natural data. Journal of Structural Geology 9 (5–6), 731–745.

Wenk, H.R., Venkitasubramanyan, C.S., Baker, D.W., Turner, F.J., 1973. Preferred orientation in experimentally deformed limestone. Contributions to Mineralogy and Petrology 38 (2), 81–114.

Wenk, H.R., Matthies, S., Donovan, J., Chateigner, D., 1998. BEARTEX, a Windows-based program system for quantitative texture analysis. Journal of Applied Crystallography 31, 262–269.

Wyckoff, R.W.G., 1920. The crystal structures of some carbonates of the calcite group. American Journal of Science 50, 317–360.